Linköping Studies in Science and Technology
Dissertation No. 2446

Simulation and Modelling of Organic Thermoelectric Materials and Devices

Najmeh Zahabi

LINKÖPING UNIVERSITY

Linköping studies in science and technology. Dissertations No. 2446

Simulation and Modelling of Organic Thermoelectric Materials and Devices

Najmeh Zahabi

Department of Science and Technology,
Laboratory of Organic Electronics

Linköping University
SE-581 83 Linköping, Sweden
Norrköping 2025

Supervisor:
Prof. Igor Zozoulenko
Laboratory of Organic Electronics, Department of Science and Technology, Linköping University

Co-supervisor:
Assoc. Prof. Glib Baryshnikov
Laboratory of Organic Electronics, Department of Science and Technology, Linköping University

Faculty opponent:
Prof. Alessandro Troisi
School of Physical Sciences, Faculty of Science and Engineering, University of Liverpool

Simulation and Modelling of Organic Thermoelectric Materials and Devices

Linköping studies in science and technology. Dissertations No. 2446

Printed in Sweden by LiU-tryck, 2025
ISBN: 978-91-8118-077-0 (print)
ISBN: 978-91-8118-078-7 (PDF)
https://doi.org/10.3384/9789181180787
ISSN: 0345-7524

Description of the cover:
The cover image is an abstract artistic representation of a thermoelectric generator, created using AI-generated visuals and further modified to enhance clarity and thematic relevance.

Abstract

As the need for autonomous and on-site renewable power sources grows, developing efficient energy solutions for distributed sensors, wearable electronics, cooling systems, and other low-power applications has become increasingly critical. Organic thermoelectric generators (TEGs), which convert low-grade heat into electrical energy through the Seebeck effect, offer a promising solution for powering these devices. Organic TEGs possess some advantages over inorganic TEGs in the context of sustainable energy harvesting because the active materials are often solution-processable at room temperature, which enables scalable patterning and printing techniques. Furthermore, these semiconductors are typically derived from Earth-abundant, non-toxic elements, making them environmentally friendly and sustainable. Among organic semiconductors, conducting polymers, particularly PEDOT (Poly(3,4-ethylenedioxythiophene)), emerge as pivotal materials in organic TEGs due to their favorable electrical and thermal properties. Thus, a deep understanding of these polymers is essential for guiding material design and optimizing device performance. In this regard, computational methods represent an important tool in studies of organic thermoelectric materials and devices since they not only provide insights into the electronic and thermal properties of materials on atomic and molecular levels but also allow for the prediction of the device's performance without the need for extensive experimental work.

This thesis employs multi-scale computational modeling to advance the understanding and optimization of organic thermoelectric materials and devices, including: (I) Finite element method modeling to analyze and optimize the micro-TEGs, (II) Ab initio molecular dynamics simulations to investigate charge transport mechanisms in PEDOT conducting polymer, and (III) Machine learning approaches to predict and study the electronic properties of PEDOT thin films.

Part (I) presents that achieving power densities in the range of mW cm−2 at a temperature gradient of 10 K is feasible through geometrical optimization and utilizing advanced organic thermoelectric inks. Particularly, we simulated the PEDOT:PSS/BBL:PEI micro-TEGs and

improved device efficiency under varying thermal gradients using COMSOL software.

In part (II), we developed a computational technique based on ab initio molecular dynamics to trace the temporal motion of charge carriers in a single PEDOT chain and in coupled chains with varying degrees of interaction. Subsequently, we used ab initio molecular dynamics to demonstrate that charge transport along the chains is band-like, while transport across chains follows a hopping-like mechanism. The calculated polaron mobility along the chains reached 4 cm2V−1s−1, providing a theoretical upper limit for thiophene-based conducting polymers. Also, we quantified the hopping rate between chains, consistent with Marcus theory, by analyzing polaron jumps.

Part (III) integrates computational modeling with machine learning to explore changes in morphological and transport properties of PEDOT:Tos prepared using different solvents. We employed convolutional neural networks to achieve high accuracy (r2>0.99) in predicting electronic coupling values and significantly accelerated the analysis compared to density functional theory calculations. This approach enabled detailed investigations into how different solvents affect the electronic coupling of PEDOT dimers.

We believe that our findings on organic thermoelectric material and devices provide a comprehensive framework for improving the performance and scalability of organic TEGs and open new avenues for further research.

Keywords: computational modeling, thermoelectric generator, conductive polymer, ab initio molecular dynamics, charge transport, machine learning

Populärvetenskaplig sammanfattning

Kan vi verkligen omvandla spillvärme till elektricitet och driva små IoT-enheter, såsom sensorer och ställdon utan batterier? Denna avhandling visar att svaret kan vara ja genom användning av organiska termoelektriska generatorer (TEGs). Dessa generatorer bygger på Seebeck-effekten, där temperaturskillnader omvandlas till elektricitet. Men vad gör organiska TEGs så speciella? Till skillnad från traditionella, oorganiska alternativ är de billiga att producera, kan tryckas direkt på flexibla ytor och består av rikligt förekommande, giftfria material. Den ledande polymeren PEDOT (Poly(3,4-ethylenedioxythiophene)) spelar en central roll i tekniken, tack vare dess utmärkta elektriska och termiska egenskaper.

Genom avancerade datorsimuleringar har denna avhandling kartlagt hur PEDOT kan optimeras för att maximera energiutvinningen. Våra studier visar att genom smart design kan dessa generatorer producera effektdensiteter i nivån mW/cm² vid temperaturdifferenser på endast 10 grader. Det innebär till exempel att en blodsockermätare kan drivas av temperaturskillnaden mellan kroppen och omgivningen, vilket eliminerar behovet av batterier.

Dessutom har simuleringar av laddningsrörelser avslöjat att elektroner i polymeren rör sig både genom bandtransport och genom hopp mellan kedjor – insikter som kan användas för att skräddarsy materialet för ännu bättre prestanda.

Ett genombrott i denna avhandling är användningen av maskininlärning för att påskynda analysen av polymerens egenskaper. Genom att träna neurala nätverk på stora datamängder kan denna metod nu förutspå elektroniska kopplingar med en nästan perfekt noggrannhet ($r^2>0.99$), vilket dramatiskt minskar behovet av tidskrävande beräkningar.

Vad betyder detta för framtiden? Tekniken kan bana väg för nya, batterilösa sensorer som drivs av kroppsvärme eller maskiners spillenergi. Tänk dig medicinska implantat som aldrig behöver laddas eller industriella system som återvinner sin egen värme för att driva elektronik. Med fortsatt forskning kan organiska TEGs bli en nyckelkomponent i framtidens hållbara energilösningar.

Acknowledgments

I would like to begin by expressing my heartfelt gratitude to all those who have supported, guided, and inspired me throughout my doctoral journey. Without their unwavering support, this thesis would not have been possible. I would like to deeply thank:

Prof. Igor Zozolenko, my supervisor, for his continuous guidance, patience, and invaluable insights throughout my research. Your expertise, encouragement, and the regular meetings we had were crucial to my progress. I am truly grateful for the wonderful doctoral opportunity you provided.

Dr. Glib Baryshnikov and Dr. Mathieu Linares, my co-supervisors, for your support, advice, and the thought-provoking discussions that helped shape the direction of my work.

Dr. Riccardo Ruralli, for supervising me during my secondment at the Institut de Ciència de Materials de Barcelona (ICMAB-CSIC). Your mentorship was invaluable during this time.

Dr. Besira Mihiretie, for supervising me and providing such a rewarding experience during my time at Hot Disk Company in Gothenburg. Your guidance made this period truly meaningful.

The members of the Theory and Modelling Group, for their collaboration, feedback, and the stimulating environment they provided. It has been a pleasure to work alongside such talented and driven individuals.

All the participants in the HORATES project, for the enriching meetings in different countries. These gatherings were not only professionally beneficial but also filled with adventure, camaraderie, and unforgettable moments of fun.

Lovisa, for the enjoyable lunch times we shared and for teaching me Swedish. Your kindness and friendship were a constant source of comfort.

Melissa, for making my final months at LOE so memorable. Your kindness, positivity, and friendship made my time there truly special and unforgettable.

Lastly, I would like to express my deepest gratitude to my family, for their constant love, encouragement, and belief in me. Your support has been my foundation, and without you, this accomplishment would not have been possible.

Norrköping, 2025
Najmeh Zahabi

List of included publications

I. Charge Carrier Dynamics in Conducting Polymer PEDOT Using *Ab Initio* Molecular Dynamics Simulations
Najmeh Zahabi, Glib Baryshnikov, Mathieu Linares, Igor Zozoulenko
The Journal of Chemical Physics
Contribution: Carrying out simulations, Analyzing and interpreting results, Visualization, Writing the manuscript

II. Band Versus Hopping Transport in Conducting Polymers by *Ab Initio* Molecular Dynamics: Exploring the Effect of Electric Field, Trapping and Temperature
Najmeh Zahabi, Igor Zozoulenko
Advanced Electronic Materials
Contribution: Carrying out simulations, Analyzing and interpreting results, Visualization, Writing the manuscript

III. A Rolled Organic Thermoelectric Generator with High Thermocouple Density
Nathan James Pataki*, Najmeh Zahabi*, Qifan Li, Pietro Rossi, Marco Cassinelli, Matteo Butti, Matteo Massetti, Simone Fabiano, Igor Zozoulenko, Mario Caironi
(*Authors contributed equally)
Advanced Functional Materials
Contribution: Carrying out the simulation part, Analyzing the data from the simulation, Writing the manuscript for the simulation part.

IV. From Solvent Baths to Charge Paths: Deciphering Conductivity in PEDOT:TOS Guided by Machine Learning
Najmeh Zahabi*, Ioannis Petsagkourakis*, Nicolas Rolland, Ali Beikmohammadi, Xianjie Liu, Mats Fahlman, Eleni Pavlopoulou, and Igor Zozoulenko
(*Authors contributed equally)

Submitted to Phys Rev Materials

Contribution: Carrying out the simulation part, Writing code, Running machine learning experiments, Analyzing and interpreting results, Visualization, Writing the manuscript

Related publications not included in the thesis

V. Anisotropic Lattice Thermal Conductivity in Highly Ordered PEDOT Fibers
Paolo Sebastiano Floris, Najmeh Zahabi, Igor Zozoulenko, Riccardo Rurali
Macromolecular Materials and Engineering
Contribution: Carrying out part of the simulation and assisting with data analysis.

VI. Fully Printed Thermogalvanic Modules for Low-Grade Energy Harvesting
Pedro Santos Candiotto de Oliveira1, Naveed Ul Hassan Alvi, Najmeh Zahabi, Filippa Wentz, Kathrin Freitag, Lars Herlogsson, Zia Ullah Khan, Igor Zozoulenko1, Reverant Crispin, Dan Zhao
Submitted to npj Flexible Electronics
Contribution: Carrying out the simulation part, Analyzing the data from the simulation, Writing the manuscript for the simulation part.

Table of Contents

Chapter 1

Introduction

Motivation and Research Background

The global energy crisis is one of the most pressing challenges of our time. With the increasing demand for power and the depletion of fossil fuel resources, the need for sustainable and renewable energy solutions has never been more critical. Traditional energy sources contribute significantly to environmental pollution and climate change, highlighting the urgent necessity for alternative, eco-friendly technologies. While solar, wind, and hydroelectric power have garnered widespread attention, there remains a substantial gap in harnessing and utilizing waste heat, which is an abundant and often overlooked energy source.

One promising solution to this challenge lies in thermoelectric generators (TEGs), which can convert heat into electrical energy through the Seebeck effect [1]. TEGs hold immense potential for applications in industrial environments and space exploration [2], [3], but they are also useful in everyday conditions. TEGs can harvest low-grade heat, making them suitable for applications with small temperature differences, such as body heat-powered wearables and ambient waste heat recovery. These devices provide a self-sustaining power source for distributed sensors, wearable electronics, and cooling systems [4]. Despite their advantages, conventional TEGs, primarily made from inorganic materials, often suffer from drawbacks such as high material costs, toxicity, and complex fabrication processes. This has driven the development of more sustainable and flexible alternatives, leading to the rise of organic thermoelectric generators (OTEGs).

Organic TEGs, particularly those based on conducting polymers such as poly(3,4-ethylenedioxythiophene) (PEDOT), offer several advantages over their inorganic counterparts. These materials are solution-processable at room temperature, enabling scalable and cost-effective manufacturing methods such as printing and patterning [5].

Additionally, organic semiconductors are typically derived from Earth-abundant, non-toxic elements, making them a more environmentally friendly choice. However, optimizing the performance of these materials requires a deep understanding of their charge transport mechanisms, morphology, and overall device efficiency.

To address these challenges, computational modeling has emerged as a powerful tool for investigating and optimizing organic thermoelectric materials and devices. Through multi-scale simulations, researchers can gain valuable insights into the electronic and thermal properties of these materials at atomic and molecular levels. Moreover, computational approaches enable the prediction of device performance, reducing the reliance on time-intensive and costly experimental work. However, despite its advantages, computational modeling often requires significant computational resources and time-consuming simulations, particularly when dealing with complex material systems or large-scale device optimizations.

In response to these limitations, machine learning (ML) has emerged as a transformative approach in material science, enabling faster and more efficient analysis of large datasets. By leveraging advanced algorithms, ML can identify patterns, predict material properties, and optimize performance with minimal computational cost compared to traditional simulations. This integration of ML with computational modeling allows researchers to accelerate material discovery, streamline optimization processes, and reduce reliance on expensive trial-and-error methods, ultimately enhancing the development of sustainable energy solutions.

Aim and Outline of the Thesis

The primary objective of this thesis is to develop and implement computational models for studying organic thermoelectric materials and devices. The research aims to enhance the understanding of charge transport mechanisms, material morphology, and device efficiency through a multi-scale computational approach. By integrating ab initio molecular dynamics (AIMD), finite element method (FEM), and machine learning (ML) techniques, this study seeks to:

1. Investigate the fundamentals of charge transport in conducting polymers, particularly PEDOT.
2. Model and optimize thermoelectric device performance using FEM simulations.
3. Accelerate the prediction of electronic properties of conducting polymer using ML methodologies.

This thesis is organized into multiple chapters, each addressing different aspects of the computational modeling and analysis of organic thermoelectric materials and devices.
The thesis starts with Chapter 1, Introduction, where the motivation behind the research is presented. This chapter emphasizes the significance of thermoelectric generators and highlights the role of organic materials in advancing sustainable energy harvesting technologies. Then, in Chapter 2, a fundamental discussion on organic electronics is provided, with a particular focus on conducting polymers. The chapter explores the charge transport mechanisms in these materials. In Chapter 3, Thermoelectrics, the principles of the Seebeck effect are introduced, along with a discussion on the efficiency criteria for thermoelectric materials and devices. After that, Chapter 4, Molecular Dynamics, provides a detailed explanation of both classical and ab initio molecular dynamics techniques. Next, in Chapter 5, the finite element method (FEM) is introduced and explains the simulation workflow using COMSOL software. Finally, Chapter 6, explores various machine learning techniques, including convolutional neural networks, and discusses their applications in material science.

The thesis concludes with a summary of the research findings in the final chapter.

In Paper I and Paper II, we focused on the fundamental charge transport mechanisms in conducting polymer PEDOT using ab initio molecular dynamics. A computational technique was developed to trace the temporal motion of charge carriers in a single PEDOT chain and in coupled chains with varying degrees of interaction. The simulations demonstrated that charge transport along the chains follows a band-like mechanism, while transport across chains exhibits a hopping-like mechanism. Additionally, we quantified the hopping rate between chains, consistent with Marcus theory, by analyzing polaron jumps. The calculated polaron mobility along the chains reached 4 $cm^2V^{-1}s^{-1}$, establishing a theoretical upper limit for thiophene-based conducting polymers.

In Paper III, we used finite element method simulations to analyze and optimize micro-thermoelectric generators. By simulating PEDOT:PSS/BBL:PEI micro-TEGs under varying thermal gradients using COMSOL software, we demonstrated that power densities in the range of mW cm^{-2} at a temperature gradient of 10 K are achievable through geometrical optimization and advanced thermoelectric ink formulations.

In Paper IV, we integrated computational modeling and experimental results with machine learning to explore changes in morphological and transport properties of PEDOT:Tos prepared using different solvents. We employed convolutional neural networks to achieve high accuracy ($r^2 > 0.99$) in predicting electronic coupling values and significantly accelerated the analysis compared to traditional density functional theory calculations. This approach allowed for detailed investigations into how different solvents influence the electronic coupling of PEDOT dimers.

Overall, our findings provide a comprehensive framework for improving the performance and scalability of organic TEGs and open new avenues for further research in computational modeling, charge transport analysis, and thermoelectric device optimization.

Chapter 2

Conducting Polymers

This chapter provides an overview of conducting polymers. We explore the principles of charge transport mechanisms in these materials, focusing on hopping and band charge transport. Finally, in the last part, the thesis focuses on PEDOT, a widely studied conducting polymer, examining its structural and electronic properties to gain deeper insights into its charge transport mechanisms.

Organic refers to compounds primarily composed of Carbon C atoms, often in combination with Hydrogen H atoms, and sometimes other elements. Hydrocarbons are the simplest form of organic compounds and are the foundation of many more complex organic molecules, which are classified based on the bonds between carbon atoms like alkanes, alkenes, alkynes, and aromatic hydrocarbons. The molecular structures of hydrocarbons are illustrated in Figure 1. Alkanes contain only single bonds between carbon atoms and follow the formula C_nH_{2n+2}, alkenes with at least one double bond, having the formula C_nH_{2n}, alkynes contain at least one triple bond between carbon atoms, following the formula C_nH_{2n-2}, and aromatic hydrocarbons contain a ring structure with alternating single and double bonds between carbon atoms, typically forming a benzene ring. These hydrocarbons are particularly stable due to their resonance structure [6].

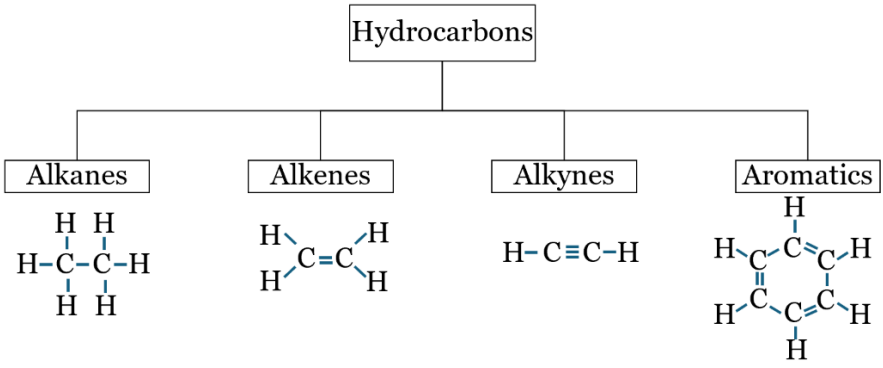

Figure 1. Diagram illustrating the four main types of hydrocarbons: alkanes (single bonds), alkenes (one or more double bonds), alkynes (one or more triple bonds), and aromatic hydrocarbons (ring structures with alternating single and double bonds, such as benzene).

Hydrocarbon molecules can create polymers through a process called polymerization, where individual monomer units (small molecules) chemically bond together to form long, repeating chains. The type of polymerization and the structure of the hydrocarbon molecules determine the properties of the resulting polymer. Hydrocarbons with alternating single and double bonds, or aromatic hydrocarbons, form conjugated polymers, which are key to conducting polymers used in electronics due to charge delocalization across the carbon-carbon bonds. This delocalization of charges is a key characteristic that enables electrical conductivity.

To be more specific, we can examine the simplest conjugated polymer, polyacetylene, which consists of alternating single and double bonds along a linear carbon chain. In such structures, the double bonds are comprised of a σ-bond and a π-bond. While the σ-bond is formed by the direct overlap of atomic orbitals along the internuclear axis, the π-bond arises from the sideways overlap of p-orbitals. This π-bonding creates a π-system, where the electrons in the p-orbitals are not confined to a single bond but are instead delocalized over the entire conjugated chain, where electrons can move freely along the polymer chain. Figure 2 shows the structure of polyacetylene, highlighting the alternating single and double bonds and the resulting π-system. This electron mobility is a critical requirement for electrical conductivity [6].

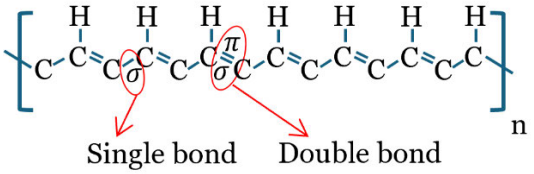

Figure 2. Structure of polyacetylene highlighting the single and double bonds along the polymer chain.

While conjugated polymers have the potential for conductivity due to their delocalized electrons, their conductivity can be enhanced through a process called doping. Doping involves introducing charge carriers (either electrons or "holes") into the polymer by adding specific chemical dopants. This increases the number of free charges available for conduction and improves the electrical properties of the polymer [7].

In 1977, Shirakawa and his colleagues, Alan J. Heeger and Alan G. MacDiarmid, demonstrated that polyacetylene, a polymer typically an insulator, could be transformed into a conductive material by introducing oxidizing agents like iodine or electrons [8]. While doping itself (especially in inorganic semiconductors) was not new before Shirakawa's work, he was the first to demonstrate doping in conjugated organic polymers to create materials with conductivity, a breakthrough that earned him and his colleagues the Nobel Prize in chemistry in 2000. This opened the door for the development of conducting polymers, a completely new class of materials with applications in electronics, sensors, and renewable energy devices. However, the ability of conducting polymers to effectively transport charge carriers, such as electrons and holes, across the polymer chain is essential for their performance in these applications [9].

Charge Transport in Conducting Polymers

In most conducting polymers, the electrical conductivity arises from the movement of charge carriers (electrons or holes) along the conjugated polymer backbone. The backbone of a conducting polymer refers to the primary chain of atoms, typically carbon, that forms the main structure of the polymer.

A key concept in charge transport within conducting polymers is the formation of polarons. When a charge carrier, such as an electron or hole, is introduced into a conjugated polymer, often through doping, it interacts with the polymer backbone. This interaction causes a local distortion in the conjugated chain, breaking the uniformity of the alternating single and double bonds. The distortion modifies the local electronic structure, creating a new energy state within the polymer's

bandgap. The charge carrier becomes "trapped" in this localized region, forming a coupled system of the charge and the surrounding distortion, referred to as a polaron. The formation of a polaron not only stabilizes the charge carrier but also allows it to move along the polymer backbone by hopping or through delocalization across adjacent molecular units [7].

Therefore, charge transport in conducting polymers is often affected by structural and energetic disorders. This leads to a range of charge transport mechanisms, including hopping conduction and band transport of charge carriers.

Hopping Transport

In the hopping transport regime, localized charge carriers, such as electrons or holes, move through the material by hopping from one site to another. These sites represent specific locations where charge carriers can reside, such as molecular orbitals, defects, or segments of a polymer chain. For hopping transport to occur, there must be an activation barrier, an energy threshold that separates one localization site from another. The charge carrier must overcome this barrier to transition to a neighboring site. This regime is typically observed in systems where charge carriers are localized, such as weakly coupled organic crystals or disordered solids like polymer melts.

Localization of charge carriers can arise from three primary mechanisms. First, the small polaron theory explains localization as a result of the interaction between the charge carrier and the surrounding medium. The charge induces a local nuclear distortion in the molecular site and its environment, stabilizing the localized charge. The resulting quasi-particle, comprising the charge carrier and the associated lattice distortion, is referred to as a small polaron. Second, nonlocal electron-phonon coupling, as proposed by Troisi and co-workers [10], [11], [12], [13], attributes localization to thermal fluctuations in the coupling between neighboring sites. This mechanism is especially relevant in systems where thermal motions dynamically alter site connectivity and charge transfer pathways. Third, in disordered systems, such as less-ordered conducting polymers, localization can occur due to static structural disorder. For

example, broken conjugation in polymer systems creates irregularities that confine charge carriers to localized regions [14], [15].

Regardless of the localization mechanism, hopping models describe charge transport in terms of charge transfer rates k_{ab} , between discrete sites a and b. These rates depend on the orbital overlap and geometries of the initial and final sites, making them highly site-specific and directionally dependent. Two important theoretical models used to calculate these hopping rates are the Marcus and the Miller-Abrahams rates.

Marcus rate models the thermally activated hopping of charge carriers by incorporating the reorganization energy, the energy required to distort the local environment to facilitate charge transfer, and the driving force, which is the energy difference between the initial and final states. This model, developed by Rudolph Marcus [16], earned him the Nobel Prize in Chemistry in 1992 for its groundbreaking application in understanding electron transfer reactions. This model is particularly relevant for systems dominated by small polaronic localization, as described earlier. Marcus theory provides a detailed, physics-based framework for understanding charge transport in disordered materials where environmental interactions are significant.

To calculate the charge carrier transfer rate between two chains based on Marcus theory, the hopping rate k_{Marcus} is expressed as:

$$K_{Markus} = \frac{2\pi}{\hbar}\frac{|H_{ab}|^2}{\sqrt{4\pi\lambda k_B T}} exp\left[-\frac{(\lambda+\Delta G)^2}{4\pi\lambda k_B Y}\right],$$

where H_{ab} denotes the electronic coupling (transfer integral) between the two sites, λ represents the reorganization energy, ΔG is the Gibbs free energy change, k_B is the Boltzmann constant, and T is the temperature. The reorganization energy λ is determined using four points on the adiabatic energy surface

$$\lambda = \left(E^{charged}_{neutral\ geometry} - E^{neutral}_{neutral\ geometry}\right) + \left(E^{neutral}_{ch\,\text{arg}ed\ geometry} - E^{charged}_{ch\,\text{arg}ed\ geometry}\right).$$

In this context, the superscripts represent whether the molecule is in a charged or neutral state, while the subscripts indicate whether the

geometry corresponds to the neutral or charged state. For further understanding, refer to Figure 3.

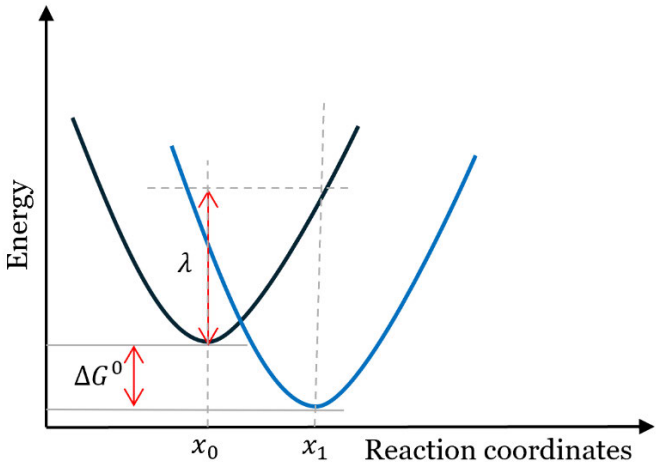

Figure 3. Schematic energy diagram illustrating Marcus theory for electron transport between localized states. ΔG^o represents the free energy change associated with transport from the initial to the final state, while λ denotes the reorganization energy required for nuclear configuration adjustments during the transport process.

The Miller-Abrahams rate [17], on the other hand, describes hopping transport in terms of the energetic differences between sites and the effect of the applied external field. This rate is computationally simpler and is especially applicable to systems where localization arises from static structural disorder, such as polymer blends or amorphous regions of conducting polymers. It focuses on how energy barriers between sites influence hopping rates, making it suitable for large-scale simulations of disordered materials.

The Miller-Abrahams rate formula, which describes hopping transport in disordered systems, is given as:

$$K_{\text{Miller–Abrahams}} = \begin{cases} k_0 |H_{ab}|^2 & if\ E_a \geq E_b \\ k_0 |H_{ab}|^2 \exp\left(\dfrac{-\Delta E_{a,b}}{k_B T}\right) & if\ E_a < E_b \end{cases}$$

where $K_{\text{Miller–Abrahams}}$ is the hopping rate, k_0 is a prefactor dependent on system-specific properties, $\Delta E_{a,b} = E_b - E_a - eFr_{a,b}$ with F being

the electric field intensity and $r_{a,b}$ the distance in the field direction between states a and b.

Band Transport

In contrast to hopping transport, band transport occurs when charge carriers, such as electrons or holes, are delocalized across the material and move freely through periodic energy bands. These energy bands arise from the underlying electronic structure of the material, which is shaped by the periodic arrangement of atoms in a crystalline lattice.

In a periodic structure, the overlap of atomic orbitals creates allowed energy levels that form continuous bands of energy, separated by forbidden gaps where no electron states exist. Electrons in these bands are not confined to a single atomic site but can move throughout the material in a wave-like manner.

Band transport is most prominent in highly ordered, ultrapure organic crystals, where strong electronic coupling enables delocalization and minimal structural or energetic disorder. However, even in these ideal conditions, charge transport is not entirely free. Carrier scattering caused by phonons (vibrational modes of the lattice) and impurities introduces resistive effects, limiting the mobility of charge carriers.

Charge Transport in PEDOT

PEDOT (Poly(3,4- ethylenedioxythiophene)) was first synthesized in 1988 by Jonas et al.[18] through the chemical oxidation of the EDOT monomer using $FeCl_3$ as the oxidizing agent. This initial breakthrough was followed by advancements in electrochemical polymerization, which diversified the synthesis strategies and expanded the application potential of PEDOT.

PEDOT's charge transport properties stem from its conjugated polymer backbone, which is a characteristic feature of conducting polymers. The structure of PEDOT and its backbone is illustrated in Figure 4. This backbone consists of alternating single and double bonds between carbon atoms, leading to a system of π-orbitals. PEDOT's backbone is nearly planar, allowing the p-orbitals to align and overlap efficiently along the chain. This overlap results in the

formation of a delocalized π-electron cloud, known as the π-system, which provides a pathway for charge carriers to move freely along the polymer.

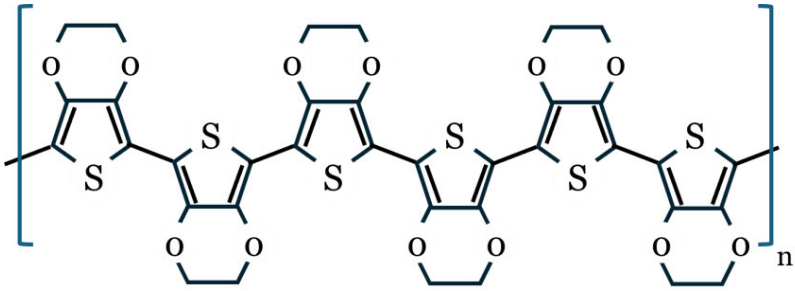

Figure 4. Schematic representation of the PEDOT polymer chain structure, with alternating single and double bonds.

The unique structure of PEDOT further enhances its charge transport potential. On top of the planarization configuration that maximizes π-orbital overlap, the oxygen atoms in the ethylenedioxy groups contribute to stabilizing the delocalized electrons. Moreover, the presence of a π-channel, PEDOT in its pristine form (i.e., polymerized PEDOT) is already highly doped, typically around 33%. This inherent doping means that PEDOT is not non-conductive like other polymers that require external doping to become conductive. However, to further enhance its conductivity, additional doping can be performed, introducing charge carriers in the form of polarons or bipolarons, see Figure 5.

Despite its promising attributes, PEDOT is inherently insoluble, which poses challenges for large-scale processing and limits its applicability. To address this, Bayer AG [19] introduced polystyrene sulfonate (PSS as the polymeric counterion to create PEDOT:PSS, a water-dispersible form of PEDOT. PSS serves as both the dopant and counterion, with its hydrophilic nature allowing PEDOT to form stable dispersions in water. This solution-processible nature, coupled with excellent film-forming properties, has made PEDOT:PSS a widely used conducting polymer in various applications, from solar cells to supercapacitors and electrochromic devices.

PEDOT can also be doped with other molecular counterions, such as chloride Cl^-, perchlorate ClO_4^-, and tosylate Tos^-. These dopants not only modify the charge distribution within the PEDOT lattice but also alter the polymer's internal structure [20].

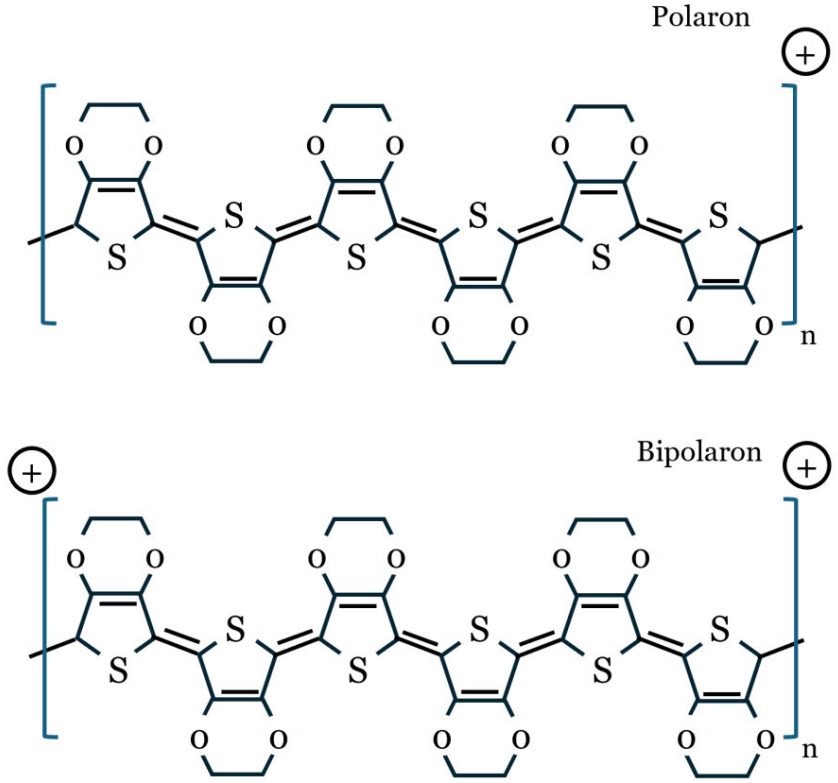

Figure 5. Schematic representation of polaron and bipolaron formations in the PEDOT structure.

Specifically, PEDOT exhibits a benzoid structure, where the C-C bonds are longer than the C=C bonds. This structural configuration limits the efficiency of charge transport along the polymer chains. However, when PEDOT is doped, the bond lengths in the polymer chains adjust, with C=C bonds lengthening and C-C bonds shortening [21]. This change leads to a transition from the benzoid structure to a quinoid structure. The quinoid structure is more planar and delocalized, enabling a stronger overlap of π-orbitals along the chain. This improved π-orbital alignment facilitates more efficient charge

transport, significantly enhancing the material's electrical conductivity.

The increase in conductivity depends on the level of doping. Heavier doping enhances percolative paths in the film, ultimately improving conductivity. For instance, PEDOT films doped via vapor-phase polymerization can achieve conductivity levels as high as 2000 S/cm, nearing metallic conductivity. Films doped with Tos^- have demonstrated even higher conductivities, exceeding 3400 S/cm [22], and some studies have reported values reaching up to 4600 S/cm for PEDOT: PSS [23].

In Papers I and II, we investigated charge transport in PEDOT chains. Specifically, in Paper 2, we examined a single PEDOT chain consisting of 24 monomer units as shown in Figure 6(a). A polaron is introduced by adding a positive charge to the system, leading to the localization of the polaron at the center of the chain (Note that Figure 5 is a schematic representation of polaron, whereas Figure 6 is actual QM calculations). Figure 6(b) depicts the carbon-carbon C-C bond length alternation for the neutral PEDOT chain (aromatic structure), while the deviation in bond lengths caused by the presence of the polaron (quinoid structure) is shown in Figure 6(c). To clarify this further, Figure 6(d) presents the individual C-C bond lengths along the PEDOT backbone in the charged state subtracted from the corresponding bond lengths in the neutral state, effectively highlighting the altered internal structure of the PEDOT chain.

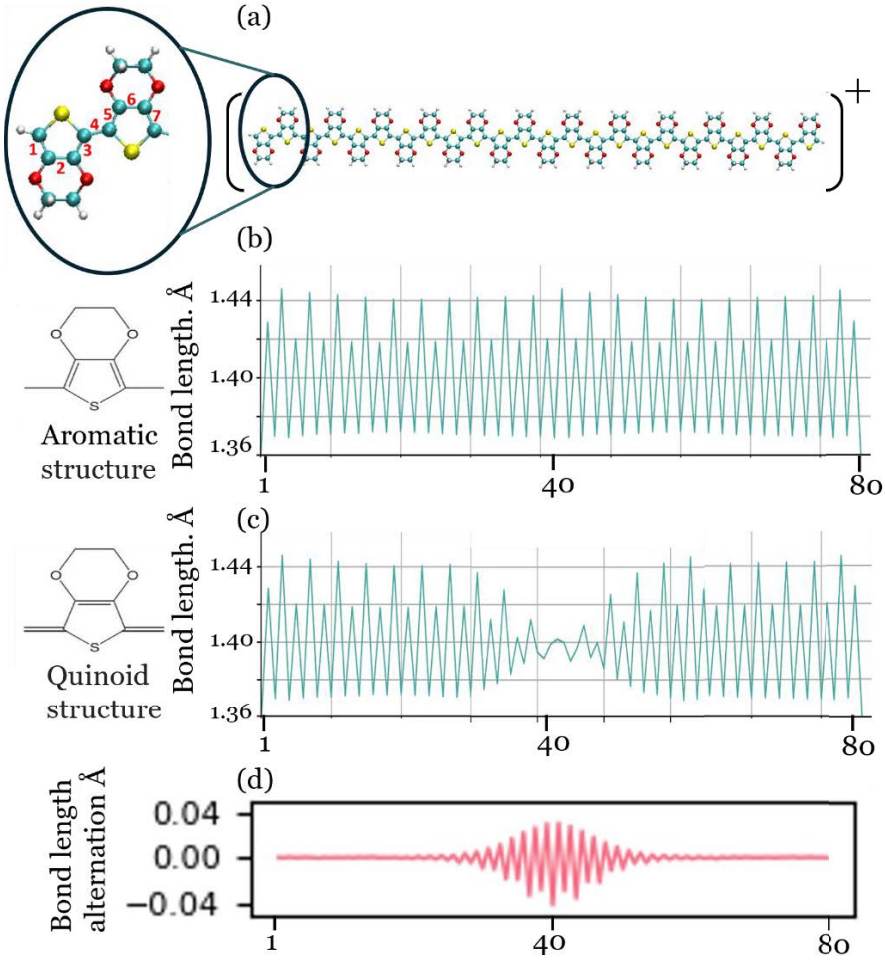

Figure 6. (a) Schematic representation of the geometrical structure of a PEDOT chain with N=24 monomers. Sulfur atoms are yellow, oxygen is red, hydrogen is white, and carbon is cyan. (b) Bond lengths of C-C bonds in neutral PEDOT. (c) Bond lengths of C-C bonds in PEDOT with a positive charge (polaron). (d) Bond length alternation, highlighting the differences between bond lengths in the neutral and polaronic states.

As explained earlier, the distortion modifies the local electronic structure, creating a new energy state within the polymer's bandgap. Figure 7 illustrates the electronic structure of the PEDOT chain, comparing the neutral and polaronic states. In the neutral

PEDOT chain, the electronic structure is defined by a well-defined energy gap between the highest occupied molecular orbital (HOMO) and the lowest unoccupied molecular orbital (LUMO). The HOMO is fully occupied, while the LUMO remains unoccupied, representing the intrinsic energy gap.

In the presence of polaron, the electronic structure undergoes significant changes. The addition of a positive charge to the system introduces localized states within the energy gap. These states, associated with the polaron, are referred to as β-LUMO in the spin-down channel (β-spin). It is energetically positioned below the unoccupied LUMO of the neutral chain but above the occupied HOMO. The introduction of these mid-gap states effectively reduces the energy gap in the polaronic PEDOT chain.

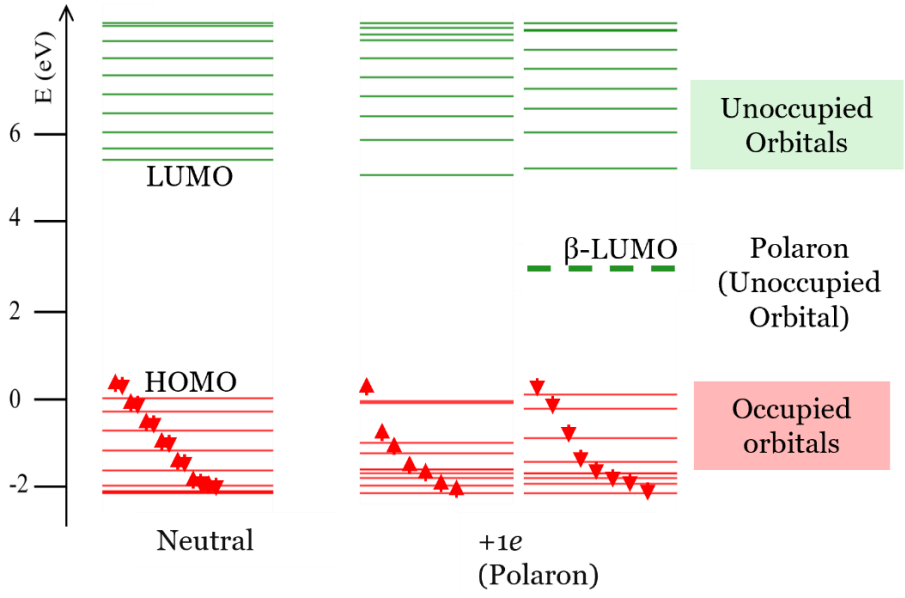

Figure 7. Electronic structure of the ground state for a neutral PEDOT chain and a chain containing a positively charged polaron. Occupied states are depicted in red, while unoccupied states are shown in green. The lowest unoccupied spin-down state represents the polaronic state.

Chapter 3

Thermoelectrics

This chapter begins with an introduction to the basic principles of the thermoelectric effect. Next, it delves into the materials used in thermoelectric applications, with a comparison of the properties of organic and inorganic materials. Particular emphasis is placed on the thermoelectric properties of PEDOT, a widely studied conducting polymer. The discussion then shifts to thermoelectric devices, highlighting their design and functionality, and concludes with an analysis of the methods and formulas used to evaluate thermoelectric efficiency.

Thermoelectric Effect

Thermoelectric Generators (TEGs) convert heat into electricity and have the potential to address the world's increasing need for sustainable energy. By efficiently harnessing low-energy-density heat sources, such as waste heat produced during the conversion of fossil fuels to electricity or heat from solar radiation, TEGs can offer a viable solution for energy recovery. The ability of TEGs to operate efficiently at low-temperature differences makes them particularly valuable for applications where traditional power generation methods are impractical, such as wearable organic electronics. TEGs generate electricity by directly converting thermal energy into electrical power through the Seebeck effect, without relying on moving parts or chemical reactions.

The Seebeck effect describes the generation of an electric voltage V across a material when a temperature gradient ∇T is applied. The Seebeck effect is mathematically expressed as:

$$J = \sigma(E - S\nabla T),$$

where J is the electrical current density, σ is the electrical conductivity, E is the applied electric field, and S is the Seebeck coefficient.

This generalized equation highlights how the electrical current density arises not only from the applied electric field but also from the thermoelectric contribution due to the temperature gradient. [24].
When a material is subjected to a temperature difference, the thermal gradient causes a redistribution of charge carriers across the material. In both n-type and p-type materials, the side exposed to higher temperatures causes charge carriers to gain thermal energy, increasing their mobility, see Figure 8. In n-type materials, where electrons are the majority charge carriers, these electrons move from the hot side (where they have higher energy) to the cold side (where they have lower energy). In p-type materials, where holes are the majority charge carriers, the holes move from the hot side to the cold side as they represent the absence of electrons and behave like positive charge carriers. This movement of charge carriers, electrons in n-type and holes in p-type, creates a voltage difference between the hot and cold sides of the material, which is the Seebeck effect [25].

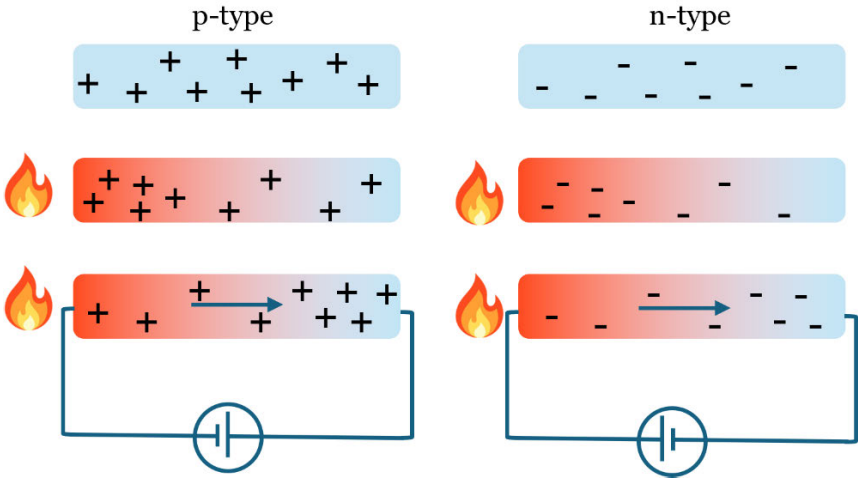

Figure 8. Schematic depiction of the Seebeck effect.

The ability of a material to transport heat and electrical currents is dictated by the values of the thermal and electrical conductivities. These two properties are essential for understanding how efficiently a material can convert thermal energy into electrical power in TEGs.

Thermal conductivity measures a material's ability to conduct heat and is influenced by factors such as its atomic structure and temperature. Materials with high thermal conductivity, such as metals, allow heat to flow easily through them, while materials with low thermal conductivity, like ceramics or polymers, resist heat flow. According to Fourier's law of heat conduction, the heat current density h is given by:

$$h = -\kappa \nabla T,$$

where ∇T is the temperature gradient, and κ is thermal conductivity. The negative sign indicates that heat flows from regions of higher temperature to lower temperature, opposing the temperature gradient. In the context of TEGs, low thermal conductivity is preferred because it helps maintain the temperature gradient across the thermoelectric material, which is necessary for efficient heat to electricity conversion. If the heat flows too easily through the material, the temperature difference between the hot and cold sides will dissipate quickly, reducing the voltage generated.

Electrical conductivity indicates how easily electric current can pass through a material. This property is governed by the density and mobility of charge carriers. High electrical conductivity is essential for maximizing the flow of electrical current in TEGs, as the electrical current is directly related to the number of charge carriers moving through the material in response to the applied voltage or temperature gradient.

For thermoelectric materials, achieving the right balance between these two conductivities is crucial. Materials that are good electrical conductors but poor thermal conductors are ideal for thermoelectric applications, as they facilitate the flow of electrical current without allowing heat to escape, thereby preserving the temperature gradient necessary for the Seebeck effect.

The performance of a TEG is characterized by the thermoelectric figure of merit ZT, which depends on the Seebeck coefficient S, electrical conductivity σ, and thermal conductivity κ of the material quantified by:

$$ZT = \frac{S^2 \sigma T}{\kappa}.$$

Maximizing *ZT* is crucial for improving the efficiency of thermoelectric materials, as it dictates the amount of electrical power that can be harvested from a given thermal gradient.

Thermoelectric Materials

Although the thermoelectric effect was discovered in the 1820s, the field of thermoelectrics gained significant attention only after the 1950s. Advancements in solid-state physics, particularly in understanding electron and phonon transport, enabled systematic studies of thermoelectric materials[26]. Notably, narrow bandgap semiconductors such as bismuth telluride (Bi_2Te_3), lead telluride (PbTe), and silicon-germanium (Si-Ge) alloys emerged as high-performance thermoelectric materials. Their high-performance stems from their ability to combine low thermal conductivity with excellent electrical conductivity [25].

Recent breakthroughs have focused on improving the dimensionless figure of merit ZT of inorganic thermoelectric materials through nano-structuring, alloying, and other innovative approaches [27], [28], [29]. These strategies aim to reduce lattice thermal conductivity without compromising electrical properties, enhancing energy conversion efficiency. While inorganic materials achieve high ZT values, they often lack mechanical flexibility and require complex manufacturing processes.

In contrast to inorganics, organic thermoelectric materials have gained attraction due to their inherent advantages, including flexibility, low cost, and ease of processing. Their potential aligns with the rising demand for wearable electronics, autonomous devices, and environmentally friendly technologies.

Organic materials entered the thermoelectric field in the 1990s, with initial studies on conducting polymers like polyaniline and polyacetylene. These materials demonstrated tunable Seebeck coefficients through doping, yet their ZT values were initially poor, typically in the range of 10^{-3} to 10^{-6}, far below those of inorganic counterparts. Since the 2000s, concerted efforts to optimize the thermoelectric properties of organic materials have led to significant breakthroughs. Researchers have achieved considerable

improvements in ZT values, particularly in conducting polymers such as Polyaniline, P3HT, and PEDOT [30], [31].

The significant progress in organic thermoelectric research can be attributed to innovative strategies aimed at optimizing their thermoelectric properties. These include controlled doping to adjust charge carrier concentration and balance electrical conductivity with the Seebeck coefficient, modifying the polymer backbone or side chains to enhance charge transport and reduce lattice thermal conductivity, integrating inorganic nanoparticles or creating hybrid organic-inorganic systems to improve both electrical and thermal properties, and reducing thermal conductivity through structural modifications or phonon-scattering mechanisms to enhance thermoelectric efficiency [4], [32], [33].

Thermoelectric Properties of PEDOT

Among organic thermoelectric conducting polymers, PEDOT stands out as one of the most promising materials due to its unique combination of properties. As a derivative of the polythiophene family, PEDOT shares characteristics such as wide-ranging high conductivity, excellent chemical stability in air, and low thermal conductivity, making it a prime candidate for thermoelectric applications.

In 2011, Bubnova et al. [30] demonstrated a significant milestone by preparing PEDOT:Tos nanofilms using spin-coating and optimizing the oxidation levels of PEDOT chains. This precise control resulted in enhanced thermoelectric performance, underlining the material's potential [34].

The thermoelectric properties of PEDOT-based materials have been extensively studied. PEDOT:PSS was first investigated for its Seebeck coefficient and electrical conductivity by Kim et al [35] in 2002. Further systematic studies on its thermoelectric performance began in 2008, with Xu's group exploring the material's potential in pellet form [36]. The addition, polar solvents such as dimethyl sulfoxide (DMSO) and ethylene glycol (EG) enhanced the electrical conductivity, yielding a ZT value of 1.75×10^{-3}. However, the low ZT

was attributed to the noncompact and disordered structure of the pellets.

To overcome these limitations, research shifted toward film structures. In 2013, Pipe et al. [37] prepared PEDOT:PSS nanofilms via spin-coating and achieved a record ZT value of 0.42 in the organic TE field. This breakthrough was achieved by simultaneously optimizing electrical conductivity and the Seebeck coefficient through DMSO dedoping. These findings highlighted the potential of PEDOT:Tos and PEDOT:PSS as leading candidates in organic thermoelectrics.

Thermoelectric Devices

A typical thermoelectric device comprises n-type and p-type materials, known as legs, arranged to form a basic π-shape element, which is the fundamental unit of a thermoelectric module. These π-shape elements are connected electrically in series and thermally in parallel to form a practical thermoelectric module, which is sandwiched between two insulator plates as shown Figure 9 [38]. Thermoelectric devices are usually a few millimeters thick and span a few centimeters in width and length.

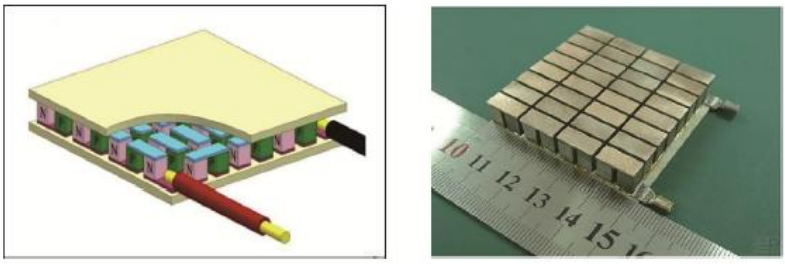

Figure 9. Structure and photograph of a thermoelectric device [38].

The basic principles of thermoelectric power generation are illustrated schematically in Figure 10.

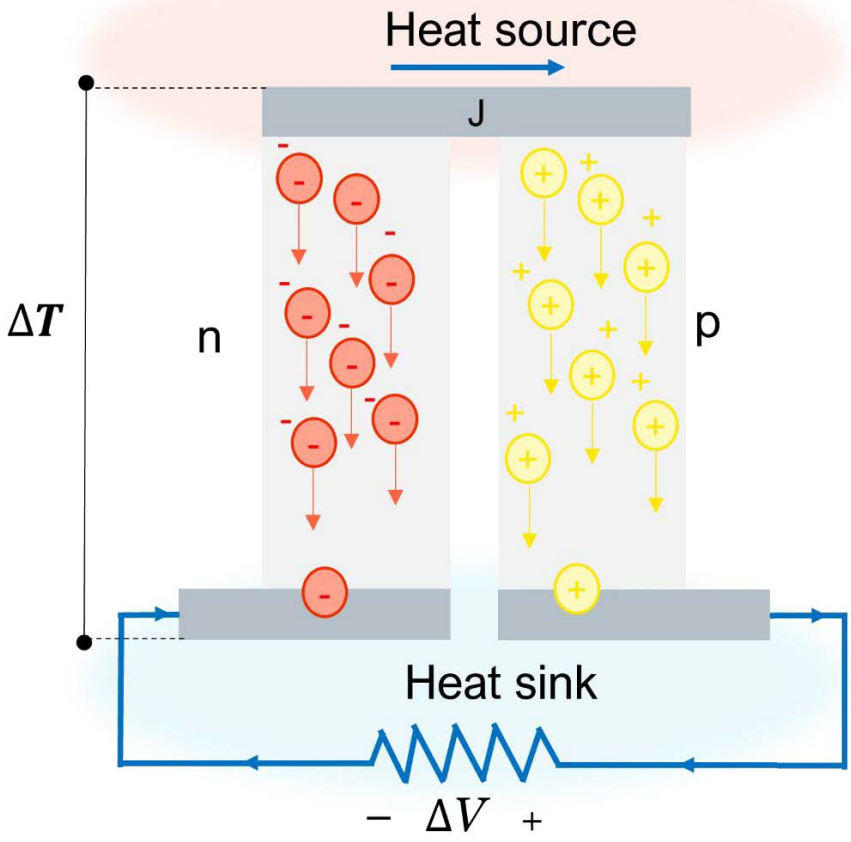

Figure 10. Schematic of a TEG illustrating p-type and n-type semiconductors arranged in a thermoelectric module. Heat applied to the hot side generates a temperature gradient, driving charge carriers and producing electrical power on the cold side.

Depending on the heat flow direction relative to the substrate and the orientation of thermocouple components, two primary configurations are employed to build a TEG: transversal (cross-plane) and lateral (in-plane). In the transversal configuration, also known as the cross-plane design, heat flows perpendicularly to the substrate surface, with the hot and cold thermocouple junctions located on separate planes. This arrangement facilitates efficient heat transfer across the thermocouples, making it ideal for scenarios requiring significant

thermal gradients. In the lateral configuration, heat flows parallel to the substrate, which hosts both the hot and cold junctions of the thermocouples. These devices employ specialized designs to optimize performance under low thermal gradients [1].

Wearable thermoelectric modules often use vertical (cross-plane) configurations to maximize temperature differences across the thermocouple junctions. This is essential to generate power effectively from small thermal gradients, such as those found in body heat. Despite the dominance of cross-plane designs, there are successful examples of planar (in-plane) configurations [1]. For instance, Francioso et al. [39] developed a flexible planar TEM using wavy-shaped polydimethylsiloxane (PDMS)/Kapton packaging, with sputtering-deposited thin films serving as the active thermocouples.

The flexibility in design and material selection enables thermoelectric devices to cater to a broad spectrum of applications, from industrial power generation to compact, wearable technologies. For example, commercially available such as the TEGpro modules are used in waste heat recovery, while devices like the Matrix PowerWatch integrate thermoelectric technology into wearable electronics .Their adaptability underscores the importance of ongoing research and development in thermoelectric materials and device engineering [40].

The commercial use of thermoelectric devices remains limited despite their many advantages [41]. This is primarily due to their low efficiency, which makes them economically uncompetitive. Improving their performance is therefore essential. Additionally, the cost of traditional thermoelectric modules per watt for cooling, heating, or power generation remains too high to replace existing technologies [48]. As a result, current thermoelectric research focuses on enhancing material performance and optimizing device design, which will be discussed in detail in the following sections.

Thermoelectric Efficiency

The efficiency of thermoelectric devices depends on accurately representing and simplifying the underlying physical processes.

First, the thermoelectric device is modeled as an idealized system, where electrical and thermal contact resistances between the electrodes and thermoelectric materials are neglected. Additionally, the thermoelectric properties of both p- and n-type materials are assumed to remain constant, irrespective of temperature variations, and the Thomson effect is disregarded. Heat transfer within the device is exclusively attributed to conduction through the TE legs, with no consideration of heat exchange via convection or radiation between the thermoelectric legs and the surrounding medium. Lastly, the Joule heat generated within the system is assumed to be evenly distributed between the hot and cold sides of the device. These assumptions provide a simplified framework to evaluate the performance and efficiency of thermoelectric systems.

Considering a thermoelectric device consisting of $2N$ legs—N p-n couples, under steady-state conditions, the heat power input Q_{in} reaches the hot side of the module, where it is transferred without loss to the cold side as Q_{out}, minus the portion converted into electrical power P.

The total voltage generated by the Seebeck effect can be expressed as:

$$\Delta V_{TEG} = S(\Delta T),$$

where S is the effective Seebeck coefficient of the material and $\Delta T = T_H - T_C$ is the temperature difference across the TEG.

When the device is connected to a load, it delivers electrical power P, determined by

$$P = I\Delta V_L,$$

where I is the current, and ΔV_L is the potential difference across the load resistance R_L:

$$\Delta V_L = IR_L.$$

The relationship between the current and voltage across the load allows for adjustments to R_L to achieve maximum power output. The open-circuit voltage ΔV_{oc} occurs at $R_L \to \infty$, and the short-circuit condition $\Delta V_L = 0$ corresponds to $R_L \approx 0$. The total voltage of the module combines contributions from individual legs. When the circuit is closed, the open-circuit voltage dissipates across R_L, and the

internal resistance R_Ω, which includes contributions from the materials and contacts:

$$2N|S|(T_H - T_C) = IR_{\Omega+}IR_{\mathrm{L}}.$$

From this, the current I is derived as:

$$I = \frac{[2N|S|(T_H - T_C)]^2}{R_{\Omega+}R_{\mathrm{L}}}.$$

Substituting I and ΔV_L into the power equation, the electrical power as a function of R_L becomes:

$$P = \frac{[2N|S|(T_H - T_C)]^2}{R_\Omega}\frac{m}{(1+m)^2}.$$

The maximum power $P_{\max}$ occurs when m=1, or $R_{\mathrm{L}} = R_\Omega$ yielding:

$$P_{max} = \frac{[2N|S|(T_H - T_C)]^2}{4R_\Omega}.$$

We now turn our attention to calculating the efficiency η of the device, employing the same assumptions used in deriving the power output. The maximum conversion efficiency can be expressed as [25]:

$$\eta_{max} = \frac{T_H - T_C}{T_H}\frac{\sqrt{1+Z_{pn}T_{avg}} - 1}{\sqrt{1+Z_{pn}T_{avg}} + \frac{T_C}{T_H}},$$

where Z_{pn} is the figure of merit of the uni-couple, T_H is the hot-side temperature, T_C is the cold-side temperature, and T_{avg} is the average temperature of the hot and cold sides. This expression highlights the interplay between the device's material properties, temperature gradients, and efficiency.

Firstly, the Carnot efficiency term $(T_H - T_C)/T_H$, underscores the importance of achieving a substantial temperature difference across the device. This reliance on $T_H - T_C$ highlights the critical role of heat exchangers and effective heat management strategies in optimizing thermoelectric performance. By maximizing the temperature difference while maintaining efficient thermal coupling, the potential for achieving higher efficiencies in thermoelectric devices is significantly improved.

Additionally, geometric configuration plays a critical role in optimizing the thermoelectric figure of merit. The optimization of Z_{pn} is achieved by satisfying the conditions:

$$\gamma_{opt} = \sqrt{\frac{\kappa_n \rho_p}{\kappa_p \rho_n}},$$

where ρ_p and ρ_n are the resistivities, κ_p and κ_n are the thermal conductivities of the p-type and n-type materials, respectively, and γ is the aspect ratios of the p-type and n-type legs, expressed as:

$$\gamma = \frac{A_p H_n}{A_n H_p}.$$

Here, A_p and A_n represent the cross-sectional area and H_p and H_n are the height of the p-type and n-type thermoelectric legs, respectively. Consequently, the maximum figure of merit, Z_{pn}^{max}, can be expressed as:

$$Z_{pn}^{max} = \left(\frac{S_p - S_n}{\sqrt{\kappa_p \rho_p} + \sqrt{\kappa_n \rho_n}} \right)^2.$$

This formulation indicates that when the p-type and n-type materials have different electrical resistivities ρ and thermal conductivities κ, the aspect ratio of the p- and n-legs must be optimized according to γ_{opt} to achieve the maximum figure of merit [25].

Chapter 4

Molecular Dynamics

This chapter begins with a brief overview of the fundamental principles of MD. It is organized into two main subsections. The first subsection discusses Classical Molecular Dynamics (MD), highlighting its computational efficiency and suitability for simulating large systems. The second subsection delves into *Ab Initio* Molecular Dynamics (AIMD), which integrates quantum mechanical calculations to achieve greater accuracy, making it ideal for studying charge transport.

Introduction to Molecular Dynamics

Computer simulation is a key tool in modern scientific research. Traditionally, research relied on theory and experiments. Theories use mathematical models to describe systems, often requiring simplifications to make calculations possible. Experiments test these theories by measuring and observing real systems. However, experiments can be limited by high costs, equipment restrictions, or challenges in reproducing extreme conditions.

Computer simulations bridge the gap between theory and experiments. They allow researchers to study systems under controlled conditions by solving mathematical models using computers. Advances in computing power and algorithms have made simulations faster and more accurate. Visualization tools also make it easier to observe and analyze simulation results. Simulations save time and cost while providing insights into systems that may be too complex or inaccessible for direct experiments.

Among various simulation methods, atomistic simulations are widely used to study systems at the atomic and molecular levels. This approach is important because the behavior of atoms and molecules determines the physical and chemical properties of materials. Atomistic simulation methods differ in complexity and accuracy. They range from simple statistical approaches to detailed quantum mechanical calculations, including Monte Carlo Simulation, Classical

MD, Coarse-Grained MD, Semiempirical Methods, and AIMD. In the following sections, we will provide a more detailed explanation of Classical MD and AIMD [41].

Classical Molecular Dynamics

Classical simulation describes the motion of atoms over time using Newton's laws of motion. Forces between atoms are calculated using empirical force fields, which are mathematical models that approximate the potential energy of the system. MD simulation provides both equilibrium and dynamic properties of systems. It is widely used in many fields, such as biology, chemistry, and materials science, to study processes like diffusion, phase transitions, and mechanical properties. Compared to quantum mechanical methods, classical MD simulation is computationally efficient and can handle larger systems.

Classical MD simulation follows a structured workflow with several key steps as shown in Figure 11.

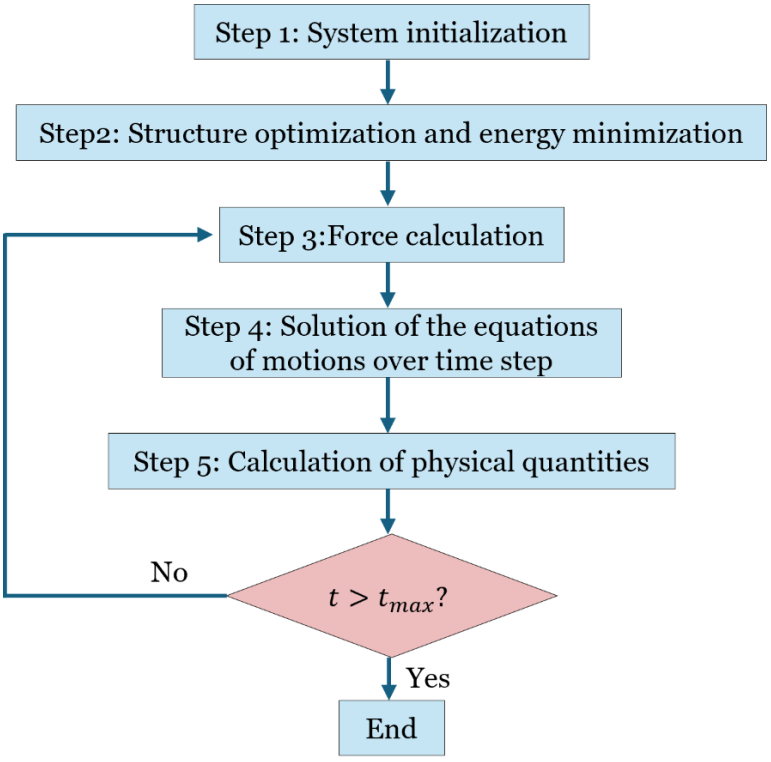

Figure 11. Flowchart illustrating the process of a classical MD simulation.

In step 1, the initial conditions for the system are established. This includes setting the positions and velocities of atoms, defining boundary conditions, and specifying any constraints. Additionally, the potential energy function, which governs the interactions between atoms, is determined.

Step 2 adjusts the initial structure to resemble an equilibrium state according to the selected potential energy function. It provides a better starting point for the simulation, leading to smoother execution. While this step is generally beneficial, it may not always be necessary. For example, if a simulation is continuing from a prior well-equilibrated state, structural optimization, and energy minimization can be skipped. However, starting from experimental data or *ab initio* calculations often requires this step because the initial structure might not be in equilibrium.

The forces acting on each atom are calculated using the potential energy function in step 3. These forces dictate how the atoms will move. Using the calculated forces, Newton's equations of motion are solved in step 4 to determine how the positions and velocities of the atoms change over a small time step.

After updating the atomic positions and velocities, physical quantities of interest, such as energy, temperature, and pressure, are computed. If the simulation time has not reached its predefined maximum, or specific conditions are not yet met, the process loops back to Step 3. Otherwise, the simulation ends.

It is important to define an MD simulation box when initializing a system. A common concern is how to handle the boundaries of the box since atoms near the boundaries may behave differently due to fewer neighbors. To avoid these "surface effects," periodic boundary conditions are often applied, see Figure 12. This method eliminates surfaces by treating the system as though it repeats infinitely in all directions. Atoms in the primary simulation box interact not only with other atoms inside the box but also with their periodic images in adjacent boxes. When an atom leaves one side of the simulation box,

its periodic image enters from the opposite side. This ensures that the number of atoms in the system remains constant.

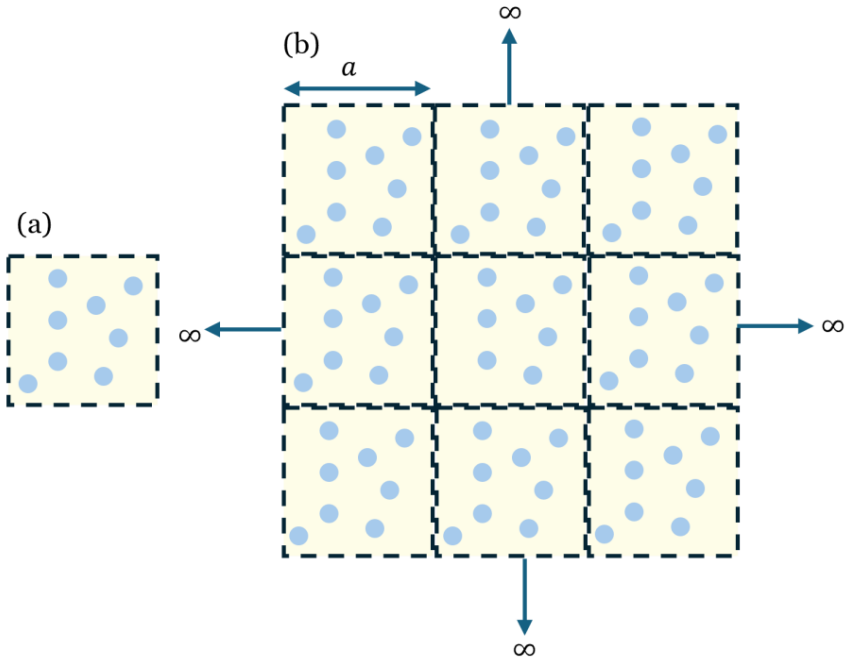

Figure 12. (a) Schematic representation of a realistic atomic system. (b) Schematic of an artificial atomic system, created by replicating the simulation cell in all three dimensions to extend it infinitely.

Classical MD relies on statistical ensembles to define the conditions of the simulation. Four major ensembles are frequently used:

Canonical Ensemble or *NVT* in which the number of atoms *N*, volume *V*, and temperature *T* are constant.

Microcanonical Ensemble or *NVE* in which *N*, *V*, and total energy *E* are constant.

Isothermal-Isobaric Ensemble or *NPT* in which *N*, *T*, and pressure *P* are constant.

Grand Canonical Ensemble or μVT in which *V*, *T*, and chemical potential μ are constant.

The system's total energy is a combination of potential energy and kinetic energy. The potential energy is derived from the potential

energy function, while the kinetic energy is determined using atomic velocities.

One key metric used in analyzing MD simulations is the radial distribution function (RDF), which measures how atomic density varies with distance from a reference atom. The physical meaning of the RDF is illustrated in Figure 13. The red sphere at the center represents the "target atom," while dN denotes the number of atoms (gray spheres) situated at distances between r and $r + dr$ from the target atom.

The RDF is then calculated as:

$$g(r) = \frac{dN}{4\rho_N \pi r^2 dr},$$

where ρ_N is the number density of the system. The RDF reveals structural information, such as how atoms are distributed around each other [42].

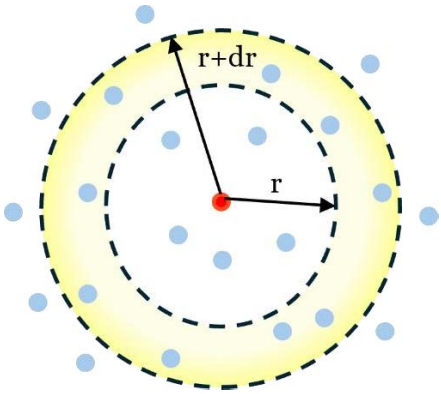

Figure 13. Illustration of the radial distribution function

While the RDF provides insights into the local structural arrangement of atoms, another essential tool for studying atomic-scale order is X-ray diffraction (XRD). XRD is calculated by determining how the atomic arrangement scatters X-rays, producing a diffraction pattern. The key to this calculation is the structure factor $F(h)$, which quantifies the interference of X-rays scattered by atoms. It is given by [42]:

$$F(h) = \sum_j f_j \exp(2\pi i h r_j),$$

where h is the reciprocal lattice vector, r_j is the position of the j-th atom, and f_j is the atomic form factor. The intensity of the diffraction pattern is proportional to the square of the structure factor:

$$I(h) = |F(h)|^2.$$

Using Bragg's law $n\lambda = 2dsin\theta$, the diffraction angles 2θ corresponding to the peaks are calculated, where d is the interplanar spacing. The resulting XRD pattern is a plot of I versus 2θ, revealing the material's crystallographic information.

Various computational tools, such as LAMMPS [43] or standalone software like Debyer, offer features for calculating XRD patterns directly from MD simulations.

Ab Initio Molecular Dynamics

AIMD uses quantum mechanics to calculate forces between atoms directly from first principles. It solves the Schrödinger equation to model the behavior of electrons and does not rely on empirical force fields. AIMD provides a very accurate description of atomic interactions, making it ideal for studying chemical reactions, electronic properties, and systems where quantum effects are important.

Despite its high accuracy, AIMD is computationally expensive and typically used for small systems of fewer than 100 atoms. Advances in computational methods and resources are gradually expanding its applications to more complex systems.

To understand how AIMD integrates both *ab initio* calculations and MD simulations, we start with the general form of the time-dependent Schrödinger equation. This equation describes a system consisting of N_n nuclei with position vectors $R^{N_n} = \{R_1, R_2, \ldots, R_{N_n}\}$, along with N_e electrons described by their position vectors $r^{N_e} = \{r_1, r_2, \ldots, r_{N_e}\}$. The time-dependent Schrödinger equation for the system is:

$$i\hbar \frac{\partial}{\partial t} \Phi(r^{N_e}, R^{N_n}, t) = H\Phi(r^{N_e}, R^{N_n}, t),$$

where $\hbar$ is the reduced Planck constant, $\Phi(r^{N_e}, R^{N_n}, t)$ is the total wave function of the system, and H is the Hamiltonian that can be expressed as

$$H = -\sum_I \frac{\hbar^2}{2M_I}\nabla_I^2 - \sum_i \frac{\hbar^2}{2m_e}\nabla_i^2 + \sum_{i<j} \frac{e^2}{4\pi\varepsilon_0|r_i - r_j|} - \sum_{I,i} \frac{e^2 Z_I}{4\pi\varepsilon_0|R_I - r_i|} + \sum_{I,J} \frac{e^2 Z_I Z_J}{4\pi\varepsilon_0|R_I - R_j|},$$

where M_I and Z_I denote the mass and the atomic number of nucleus I, respectively; m_e denotes the mass of an electron, e denotes the elementary electron charge. The first two terms represent the kinetic energy terms for both the nuclei and electrons and the last three terms represent electron-electron, electron-nucleus, and nucleus-nucleus interaction.

However, solving this equation exactly for systems with multiple interacting nuclei and electrons is infeasible due to the many-body problem. This problem arises because the wave function depends on all the positions and momenta of the particles, leading to computational demands that grow exponentially with system size.

In order to solve this equation, various approximations and methods have been developed, including the Ehrenfest method, Born-Oppenheimer approximation, Car-Parrinello approximation, and atom-centered density matrix propagation. Each method simplifies the problem in a unique way to enable simulations.

Ehrenfest MD is one of the oldest approaches in AIMD. It bridges quantum mechanics and classical mechanics by treating the nuclei as classical particles and the electrons as quantum mechanical entities.

The Ehrenfest MD approach starts with the time-dependent Schrödinger equation for the electronic wave function [42]:

$$i\hbar\frac{\partial}{\partial t}\Psi(r^{N_e}, t) = H\Psi(r^{N_e}, t).$$

The nuclei, on the other hand, follow Newtonian mechanics:

$$M_I\ddot{R}_I(t) = -\nabla_I V_E(R^{N_n}, t),$$

where $V_E(R^{N_n}, t)$ is the effective potential energy and ∇_I is the gradient with respect to the nuclear position. In Ehrenfest MD, the electronic structure problem is solved using simultaneously solving both equations for nuclei and electrons.

Another approach is the Born-Oppenheimer approximation, which relies on the significant mass difference between nuclei and electrons. Since nuclei are much heavier, their motion is much slower compared to the motion of electrons. Consequently, electrons are assumed to instantaneously adapt to the nuclear configuration at each time step, and nuclear motion is described on a potential energy surface derived from the electronic ground state. This separation allows for the time-dependent Schrödinger equation of electrons to be replaced by a time-independent Schrödinger equation.

At each nuclear configuration R^{N_n}, the electronic wave function is determined by solving:

$$H_e\psi_e(r^{N_e}; R^{N_n}) = E_e(R^{N_n})\psi_e(r^{N_e}; R^{N_n}).$$

The nuclei move on the ground-state according to classical Newtonian mechanics:

$$M_I\ddot{R}_I(t) = -\nabla_I V_E(R^{N_n}).$$

This equation describes the forces acting on the nuclei as gradients of the ground-state energy. Then the positions and velocities of the nuclei update using classical equations of motion.

Unlike Ehrenfest MD, Born-Oppenheimer MD avoids averaging over multiple electronic states, making it suitable for systems where non-adiabatic effects are negligible. However, the need to solve the electronic Schrödinger equation at every time step can be expensive, particularly for large systems. Moreover, Born-Oppenheimer MD assumes the system remains in the electronic ground state and cannot capture transitions between electronic states (e.g., excitation, charge transfer).

To address some of these limitations, Car-Parrinello Molecular Dynamics (CPMD), introduced by Car and Parrinello in 1985 [44], offers an alternative approach that integrates the electronic and nuclear degrees of freedom in a unified framework. The fundamental idea is to transform the adiabatic separation of fast electronic and

slow nuclear motions (inherent in the quantum mechanical framework) into a classical mechanical problem using an extended Lagrangian formulation.

The CPMD approach introduces "fictitious dynamics" to the electrons using orbital velocities ψ_i and a "fictitious mass" parameter μ_i, allowing the electronic system to follow the nuclear motion adiabatically. The method employs an extended Lagrangian expressed as [45]:

$$L_{CP} = \sum_R \frac{1}{2} M_I \dot{R}_I^2 + \sum_i \mu \langle \dot{\phi}_i | \dot{\phi}_i \rangle - \langle \Psi_0 | \mathcal{H}_e | \Psi_0 \rangle + \sum_{ij} \Lambda_{ij} \left(\langle \dot{\phi}_i | \dot{\phi}_i \rangle - \delta_{ij} \right),$$

where the first two terms are kinetic energy, the third term is potential energy, and $\Lambda_{ij}$are Lagrange multipliers ensuring orthonormality of the electronic orbitals.

CPMD efficiently captures the dynamic coupling between electrons and nuclei without requiring a full optimization of the electronic wave function at every MD step, as is necessary in Born-Oppenheimer MD. This reduces computational overhead in many scenarios.

In a similar way, Atom-Centered Density Matrix Propagation (ADMP) [46] provides an alternative approach to performing AIMD simulations. ADMP integrates quantum mechanical calculations into classical dynamics, similar to CPMD, but with distinct differences in its formulation and implementation. ADMP is based on propagating the electronic density matrix in time, coupled to the nuclear motion, instead of wavefunctions or orbitals.

One of the key features of ADMP is its maintenance of the idempotency and orthonormality of the density matrix during the simulation, achieved through Lagrange multipliers or penalty functions. This approach eliminates the need for frequent re-optimization of the electronic structure, making ADMP computationally efficient in many scenarios. Additionally, it is particularly well-suited for localized or Gaussian basis sets, as opposed to the plane wave basis sets commonly used in CPMD. This flexibility broadens its applicability, especially in systems where localized orbitals are advantageous.

Chapter 5

Finite Element Method and Simulation Using COMSOL Software

This chapter outlines the fundamentals of the Finite Element Method (FEM) and its application in thermoelectric modeling using COMSOL Multiphysics. It begins with an overview of FEM principles, including domain discretization, solver types, and the role of boundary conditions. The chapter then describes the simulation workflow in COMSOL, covering geometry creation, material assignment, meshing, solver configuration, and result visualization. Finally, it discusses the modeling of thermoelectric modules, focusing on the governing equations for heat transfer and electric current, demonstrating COMSOL's capability to handle coupled physics problems effectively.

Overview of the Finite Element Method

FEM is a numerical technique widely used for solving partial differential equations that describe complex physical phenomena. It is especially effective for problems involving irregular geometries, heterogeneous materials, and non-linear behaviors.

In FEM, the problem domain is discretized into smaller, simpler parts called finite elements, typically triangles or quadrilaterals in 2D and tetrahedra or hexahedra in 3D. These elements are connected at points called nodes, and the governing equations are approximated using basis functions over these elements.

Once the problem is discretized, the choice of solver becomes crucial for both efficiency and accuracy, particularly for large-scale problems. FEM solvers can be broadly classified into direct solvers and iterative solvers. Direct solvers compute the solution in a finite number of steps, offering high accuracy and robustness. They are especially effective for problems with small to moderately sized systems.

Iterative solvers are based on successive approximations, progressively refining an initial guess until convergence. These

methods are particularly suitable for large, sparse systems arising from FEM discretization. Common iterative methods include Conjugate Gradient, Generalized Minimal Residual, Bi-Conjugate Gradient, Multigrid Methods.

Another important aspect of FEM that influences the accuracy and relevance of the solution is the application of boundary conditions as they define how the system interacts with its surroundings. Mathematically, they specify the behavior of the field variables (e.g., displacements, temperatures) on the boundaries of the domain. They are generally classified into three main types: Dirichlet, Neumann, and Robin boundary conditions [47], [48].

Dirichlet boundary conditions, also referred to as essential boundary conditions, define the value of the field variable on the boundary of the domain. For example, in thermal analysis, a Dirichlet condition might set the temperature along a boundary to a fixed value, such as $T = T_0$, where T_0 is a constant temperature.

Neumann boundary conditions, also called natural boundary conditions, specify the value of the derivative (or flux) of the field variable normal to the boundary. In heat transfer, a Neumann boundary condition represents a specified heat flux at the boundary, which is the rate of heat flow through that boundary. For example, it could specify the temperature gradient at the boundary, such as zero heat flux at an insulated surface or a constant heat flux at a surface where heat is being added or removed.

Robin boundary conditions, often referred to as mixed boundary conditions, combine elements of both Dirichlet and Neumann conditions.

The FEM is implemented in various software, such as ANSYS, ABAQUS, and COMSOL software, which excels in solving coupled physics problems.

Simulation Workflow in COMSOL Software

COMSOL software is a versatile simulation platform that supports both single-physics and multiphysics modeling. The software's "Model Builder" provides an intuitive workflow for defining geometries,

specifying material properties, assigning physics, computing results, and post-processing data, see Figure 14. This structured environment ensures that even complex simulations can be tackled efficiently.

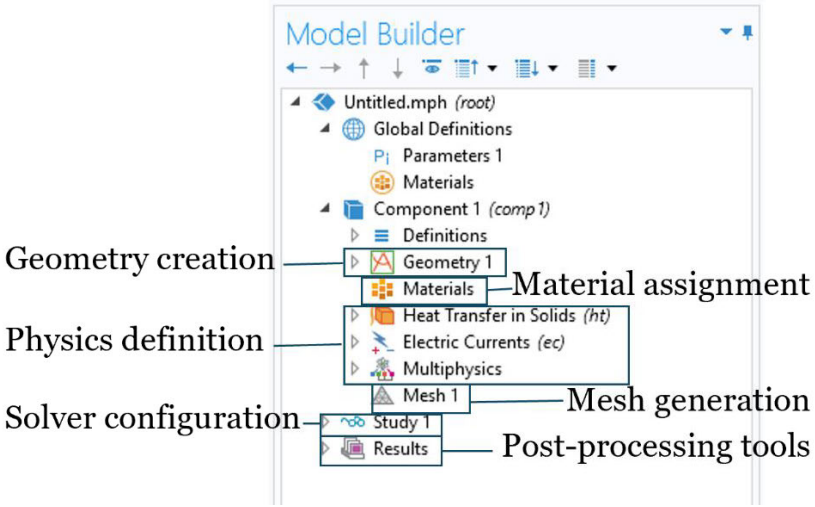

Figure 14. Screenshot of the COMSOL software "Model Builder" interface, showcasing the step-by-step workflow for simulation setup, including geometry creation, material assignment, physics definition, mesh generation, solver configuration, and post-processing tools.

To fully utilize the capabilities of this platform, it's important to understand the systematic modeling workflow. Below is a step-by-step guide to setting up and running a simulation in COMSOL Multiphysics.

Begin by initializing the simulation workspace. Choose the spatial dimensions (1D, 2D, or 3D), physics interfaces, and any additional modules required for your model. This foundation guides the subsequent modeling steps.

Geometry creation is a critical step in simulation. In COMSOL software, one can draw directly within the software using built-in tools for common shapes. For more advanced geometries, tools such as Boolean operations, transformations, and partitioning are available to refine designs, ensuring precision and accuracy. Alternatively, users can import CAD files for more intricate designs or utilize *LiveLink*™ products to connect with external CAD software.

Once the geometry is established, the next step is assigning materials to the model. This can be done by selecting from the software's extensive library or defining custom materials. Next, selecting the appropriate physics interface (e.g., heat transfer, structural mechanics, or fluid dynamics) and applying the relevant boundary conditions defines how the model interacts with its environment.

Once the materials and physics are defined, the next step is mesh generation. By generating the mesh, the geometry is discretized into smaller elements to facilitate the computation process. To create the mesh, COMSOL Multiphysics offers an option to automatically generate a physics-controlled mesh, providing a convenient and optimized solution for most scenarios. Alternatively, a custom mesh can be manually created to allow precise control over the element size, shape, and density, tailoring it to specific modeling requirements. A well-constructed mesh is critical as it balances computational efficiency with solution accuracy.

After the mesh is prepared, the simulation is run using the built-in solvers in COMSOL software. During this process, it is essential to monitor the computations to ensure everything is running smoothly. If convergence issues occur or performance optimization is needed, adjustments to the solver settings can be made to improve the results.

The final step involves postprocessing, where the simulation results are analyzed and visualized. The software provides a range of visualization tools, including color maps, contour plots, and streamlines, which effectively illustrate the physical phenomena occurring within the model. These tools enable the identification of critical factors such as heat distribution, structural stress, or fluid flow patterns.

Thermoelectric Module in COMSOL Software

Thermoelectric modules leverage the Seebeck effect to transfer heat between two sides of the module. These modules can operate as thermoelectric coolers or heaters depending on the direction of the electric current. The thermoelectric mechanism in these modules is governed by the Seebeck effect, Joule heating, thermal conduction, and electric current.

The heat transfer equation, including the effects of thermal conduction, convection, and internal heat sources, is given by:

$$\rho C_p u \cdot \nabla T + \nabla . q = Q + Q_{ted},$$

where ρ is the density of the material, C_p is the specific heat capacity, u is the velocity field (for convection), T is the temperature, Q represents volumetric heat sources, Q_{ted} is the heat generation due to thermoelectric effects, and q is the heat flux vector, which follows Fourier's law:

$$q = -\kappa \nabla T,$$

where κ is the thermal conductivity.
Combining these, the heat transfer equation becomes:

$$\rho C_p u \cdot \nabla T + \nabla . (k \nabla T) = Q + Q_{ted}.$$

Alongside heat transfer, the electric current equation describes the conservation of charge and is expressed as:

$$\nabla \cdot J = Q_{j,v},$$

where J is the current density, defined as:

$$J = \sigma E + J_e,$$

where σ is the electrical conductivity, E is the electric field, and J_e is the thermoelectric current density.
E is related to the electric potential V as:

$$E = -\nabla V.$$

J_e accounts for the thermoelectric contribution and is given by:

$$J_e = -\sigma S \nabla T,$$

where S is the Seebeck coefficient.
Substituting these into the conservation equation yields:

$$\nabla \cdot (\sigma(-\nabla V) - \sigma S \nabla T) = Q_{j,v}.$$

This equation links the electric potential V, temperature gradient ∇T, and current density J.

Chapter 6

Machine Learning

This chapter begins with an introduction to the fundamentals of ML, outlining key concepts and techniques. The chapter then shifts focus to Convolutional Neural Networks (CNNs). Finally, the chapter explores the applications of ML in material science, particularly in understanding charge transport properties in materials.

Introduction to Machine Learning

ML is a branch of artificial intelligence that focuses on building systems capable of learning from data and improving their performance over time without being explicitly programmed [49]. Unlike traditional programming, ML models learn from experience, continuously improving as they are exposed to more data. This ability to adapt and make intelligent decisions makes it useful in different industries, from healthcare and finance to entertainment and transportation. Additionally, ML has significant applications in material science, where it helps in discovering new materials, optimizing material properties, and accelerating the development of advanced technologies.

The process of building ML models involves training, where algorithms learn from labeled data (training sets) to make predictions. Each data sample consists of features (x) and corresponding labels (y). After training, models are tested on separate testing data to assess their predictive accuracy. The key objective is for the model to generalize well to new (unseen) data, ensuring effective performance beyond the training set. [50].

ML encompasses a variety of techniques and algorithms that enable computers to learn from data and make predictions or decisions without explicit programming. These techniques are broadly categorized into supervised learning, where the training data includes labels (e.g., classification and regression), and unsupervised learning, which works with unlabeled data (e.g., clustering).

In supervised learning, regression predicts continuous outcomes by modeling relationships between input features and target variables, with linear regression being a common approach. Classification, on the other hand, predicts categorical labels, using algorithms such as logistic regression, decision trees, and support vector machines. In unsupervised learning, clustering groups similar data points based on patterns or intrinsic characteristics, uncovering hidden structures in applications like customer segmentation and image compression.[51].

Building on these foundational ML techniques, deep learning takes ML to the next level by leveraging artificial neural networks to model and solve highly complex problems. Unlike traditional ML methods that often rely on manual feature extraction, deep learning automatically learns hierarchical patterns and representations from raw data, making it particularly powerful for tasks involving large datasets and unstructured data such as images, audio, and text. For example, CNNs are widely used for image-related tasks

Convolutional Neural Networks

CNN is a deep learning model that is particularly effective for analyzing data that has a grid-like structure, such as images. The process begins with the convolutional layer. These layers apply convolutional filters (kernels) to the input data. Each filter is responsible for detecting a specific pattern or feature in the image, such as edges, textures, or shapes. More filters allow the network to capture more information, but it also increases the computational load.

As the filter slides across the image, it performs a mathematical operation called convolution. This involves multiplying the values in the filter with the values in the corresponding part of the image and summing them up. The filter slides according to a parameter called the stride, which determines how far the filter moves in each step. A stride of 1 means the filter moves one pixel at a time, while a larger stride skips more pixels, resulting in a smaller feature map. Additionally, the size of the feature map can be controlled by using padding, which adds a border of zeros around the input image.

Padding ensures that the spatial dimensions of the feature map are preserved, especially when the filter size is larger than 1.
The result of the convolution is a single number, which represents how well that filter matches the pattern in that part of the image. The output of this process is a new grid called a feature map. This feature map is smaller than the original image (unless padding is used) but highlights where specific patterns are found.
After the convolution operation, an activation function, typically ReLU (Rectified Linear Unit), is applied to introduce non-linearity into the model, which is essential for learning complex patterns and relationships in the data. Without this non-linearity, the network would only be able to learn linear mappings, which are insufficient for most real-world tasks.
Once the activation function is applied, the resulting feature maps are often subjected to a pooling operation. Pooling layers are used to down-sample feature maps, reducing their spatial dimensions while retaining the most important information. The most common type is Max Pooling, which selects the maximum value from a region of the feature map.
Following the convolutional, activation, and pooling layers, the processed data is passed through additional layers to further refine the learned features. One such layer is the Dropout Layer, which is a regularization technique designed to prevent overfitting. During training, Dropout randomly disables a fraction of neurons in the layer by setting their output to zero. This forces the network to learn more generalized and robust features by not relying too heavily on specific neurons.
Finally, the output from the previous layers is flattened into a one-dimensional vector and passed to the Fully Connected Layers. These layers combine all the learned features and produce the final output. Fully connected layers are responsible for high-level reasoning, as they aggregate and interpret the features extracted in earlier layers [52], [53], [54].

Machine Learning in Material Science

The integration of artificial intelligence into materials science is revolutionizing the discovery, development, and optimization of advanced materials. Traditionally, materials science has depended on slow, resource-intensive trial-and-error in both computational and experimental methods. However, with ML and deep learning algorithms, researchers can leverage advanced computational tools to analyze data, predict material properties, and expedite the discovery process.

These computational approaches enable rapid screening of chemical spaces, uncover hidden correlations in material behavior, and guide the tailored design of materials with custom functionalities. ML techniques have demonstrated transformative impacts across diverse areas such as structural materials, functional materials, nanomaterials, and biomaterials.

To further accelerate innovation, the United States launched the Material Genome Initiative (MGI) in 2011 [55]. The MGI encourages researchers to move away from trial-and-error approaches and focus on designing materials using smarter methods. This includes creating large databases of material data, building advanced computing platforms, and using high-throughput techniques to screen materials more efficiently. The goal is to lower research costs and accelerate the development of new materials.

For example, Paul Raccuglia suggested that a predictive model could be trained using data from failed experiments. He used information from less successful hydrothermal synthesis reactions to teach a ML model how to predict the crystallization of vanadium selenite crystals. The results showed that this model performed much better than traditional manual analysis. In fact, the model was able to predict the conditions needed to create new organic-templated inorganic materials with 89% accuracy [56].

Today, there are numerous open-source databases available that researchers can easily access and utilize, such as the Harvard Clean Energy Project [57], the Open Quantum Materials Database [58], and the Materials Project [59]. For example, Kamal Choudhary's team established a criterion to identify 2D materials based on comparison

of lattice constants obtained from experiments and the Materials Project database [60].

After that, the Genome project illustrates the power of data-driven approaches in accelerating discovery [61]. The GNoME project focuses on systematically mapping the "genome" of materials, similar to how the human genome maps DNA. By using cutting-edge ML algorithms and computational methods, this project creates comprehensive databases that describe how materials behave under various conditions and how their properties can be fine-tuned for specific applications. The discovery of 2.2 million materials by GNoME, which is equivalent to about 800 years' worth of knowledge, demonstrates an unprecedented scale and accuracy in predictive capabilities.

Machine Learning Descriptors for Material Science

Descriptors play a critical role in modern materials science, particularly in the context of ML and computational materials design. These descriptors serve as numerical representations of materials' structure, composition, and properties, transforming complex material systems into formats that can be processed by ML algorithms. By effectively capturing the essential characteristics of materials, descriptors enable predictions and insights that would be difficult or impossible to obtain using traditional experimental methods alone.

Descriptors in material science can be classified into various categories based on the specific properties they aim to represent. One key category is composition-based descriptors, which describe the elemental composition of a material. For example, in a material like steel, descriptors could include the percentage of elements like iron, carbon, chromium, and other components. Another important category is structural descriptors, which are based on the arrangement of atoms within the material. These descriptors can provide information such as coordination numbers, which represent the number of nearest neighbors of an atom, as well as bond lengths and crystal symmetries. On the other hand, electronic descriptors focus on the electronic properties of materials, such as band gaps, density of states (DOS), and electronic energy levels.

One particularly important descriptor in materials science is the Coulomb matrix. This descriptor is widely used in computational chemistry and materials science to represent molecules and materials in a form that can be processed by ML models.

The Coulomb matrix is a square matrix that encodes the electrostatic interactions between the atoms of a molecule or material. For a molecule with N atoms, the Coulomb matrix has dimensions $N \times N$, where each element Mij (for $i \neq j$) represents the Coulomb interaction between atoms i and j and the diagonal elements Mii represent the self-interaction of atom i.

The formula for the Coulomb matrix elements is as follows:

$$Mij = \begin{cases} 0.5 \cdot Z_i^{2.4} & i = j \\ \dfrac{Z_i - Z_j}{|r_i - r_j|} & i \neq j \end{cases},$$

where r_i and r_j are the positions of atoms i and j, and Z_i and Z_j are their respective atomic numbers.

Machine Learning in Charge Transport

ML is increasingly transforming the landscape of materials science by offering innovative solutions to address computational challenges and accelerate discovery. In the domain of organic semiconductors, ML shows great promise in tackling the computational bottlenecks associated with predicting charge carrier mobility which is a critical parameter for electronic applications.

Specifically, charge carrier mobility in organic semiconductors is highly dependent on molecular structure and is typically governed by a hopping mechanism through spatially and energetically disordered states. Accurate prediction of mobility often relies on theoretical frameworks such as the Marcus model, which demands the calculation of charge transfer integrals and molecular energetics. These calculations, when performed through first-principle methods, are computationally expensive, especially for amorphous thin films characterized by large structural disorder.

ML provides an opportunity to alleviate these computational challenges by developing surrogate models that can predict charge transfer properties with high efficiency and accuracy. For instance,

Lederer et al. used kernel ridge regression (KRR) to predict transfer integrals in thermally disordered pentacene crystals by leveraging system-specific geometric features [62]. This approach achieved accurate mobility anisotropies that aligned well with experimental results, highlighting the effectiveness of tailored features for specific systems. Similarly, Çaylak et al. employed a deep feedforward neural network to predict transfer integrals between Alq3 molecules using the full Coulomb Matrix as input [63]. Their predictions were used to calculate charge mobilities, although the study did not analyze angular dependencies, which are crucial for fully capturing the behavior of transfer integrals. Wang et al. also explored the use of KRR with Gaussian and Laplacian kernels to predict transfer integrals in ethylene molecules [64]. While moderate accuracy was achieved, the model's performance was sensitive to feature selection. When the same ML framework was applied to naphthalene, it resulted in considerably larger errors, emphasizing the challenges of generalizing ML models to different systems. Furthermore, this study found that very large training datasets, on the scale of 200,000 dimers, were necessary to achieve good accuracy, highlighting the data-intensive nature of ML-based charge transport predictions. These examples demonstrate the potential of ML to accelerate simulations but also underline its reliance on high-quality data, and careful feature engineering. Rinderle et al. expanded the application of ML to multiscale simulations of charge transport in organic thin films, using pentacene as a test system [65]. They utilized MD simulations to generate realistic thin-film structures and extracted a dataset of dimers for analysis. Another application of ML in multiscale modeling was demonstrated for PEDOT:PSS films, combining classical and quantum mechanical simulation tools with ML to study nanoscale morphology and electronic properties by Friederich et al [66].

Chapter 7

Summary of the Papers

Paper I

In this paper, we investigate charge transport in archetypical conducting polymer PEDOT, focusing on temporal polaron dynamics. While previous studies of the temporal polaron dynamics have utilized semi-empirical or model Hamiltonians, there is currently a noticeable absence of a detailed description of polaron dynamics in polymer chains using *ab initio* methods. At the same time, *ab initio* methods, such as density functional theory (DFT) have de-facto become the methods of choice in theoretical material chemistry. Our study addresses this research gap by developing and applying a novel computational approach based on the first-principle methods, specifically the Car-Parrinello molecular dynamics (CPMD). Our analysis primarily focuses on intrachain polaron motion within a single chain and interchain motion within two coupled chains with different degrees of coupling. Furthermore, we explore the influence of temperature on polaron dynamics.

In our model we first initiate a positively charged polaron (compensated by a negative counterion) at the one end of the chain, and subsequently displace the counterion to the other end of the chain and trace polaron dynamics in the system by monitoring the bond length alternation in the PEDOT backbone and charge density distribution. We find that at low temperature (T = 1K) the polaron distortion gradually disappears from its initial location and reappears near the new position of the counterion. At the room temperature (T = 300 K), we find that the distortions induced by polaron, and atomic vibrations are of the same magnitude, which makes tracking the polaron distortion challenging because it is hidden behind the temperature-induced vibrations.

We believe that our study, based on the first principle quantum mechanical calculations, contributes to a deeper and new understanding of charge transport in conducting polymers. In particular, our findings call into question a traditional semi-empirical picture of a polaron at the room temperature as the well-defined bond alternations extended over several monomer units in the polymer chain not affected by atomic vibrations. Also, our novel computational technique opens new avenues for further research. In particular, the developed approach can be used to study polaron mobility along and between the chains, investigate charge transport in highly doped polymers, and explore other flexible polymers, including n-doped ones.

Paper II

Conductive polymers, notably poly(3,4-ethylenedioxythiophene) (PEDOT), are gaining prominence as viable organic semiconductors across diverse fields and industries, including displays, electronics, renewable energy, sensing, and thermoelectricity to name a few. Consequently, comprehensive understanding of the charge transport mechanisms in these materials has become a focal point of research attention providing valuable insights into enhancing charge carrier mobility and, consequently, advancing device and materials performance and development.

Despite the progress in unraveling the transport mechanisms in conducting polymers achieved during recent decades, there are still fundamental questions whose understanding remains elusive and represents a subject of intensive debates. One of such questions is the interplay between two distinct transport mechanisms, namely the band transport and the hopping transport, and clarifying the related temperature dependence of the conductivity in these materials. Another question of the great fundamental and practical importance is the understanding and the rational engineering of polymer-dopant interactions. Indeed, on one hand, doping proves to be an effective strategy for tuning charge density and enhancing charge transport performance by elevating the concentration of charge carriers. At the

same time, the increase in the carrier concentration introduces Coulombic traps due to electrostatic interactions with carriers localized in intrinsic hopping sites, leading to a decrease in charge carrier mobility. Can one therefore achieve a regime when the electron density is sufficiently high, and, at the same time, charges are not trapped by dopants?

To date, theoretical studies on charge transport in conductive polymers have predominantly employed *time-independent* approaches. Recently, we developed an *ab initio* molecular dynamics technique that is in position to trace *time-dependent* dynamics of charge carriers (polarons) in conducting polymers. Using this approach one can gain microscopic insights into the temporal dynamics of polarons utilizing the first-principle density functional theory approach, - i.e. at the level of the theory that has not been possible before. By applying this novel technique and directly tracing the temporal polaron dynamics, in the present study we demonstrate that transport along the polymer chains exhibits band-like behavior, whereas transport across the chains is hopping-like and temperature-induced. Hence, our calculations provide the pivotal contribution to the clarification of the fundamental question of the band vs hopping transport in conducting polymers.
Directly tracing the charge motion along the chains, we were able to provide a theoretical limit for charge mobility along the chains in thiophene-based conducting polymers (μ = 4 cm^2/Vs), - the results that we believe is of the great importance to this field. Also, our findings offer a completely new perspective on the effect of the electric field of polaron dynamics. Namely, we discover two distinct regimes of intrachain polaron movement: at the low/intermediate electric field a polaron moves with a constant velocity where charge and lattice distortion remain coupled to each other, and at the high electric fields the charge and lattice distortion become decoupled. We also explored whether the electric field could release polaron from a Coulomb trap, and we found that the required field strength is too high and exceeds typical values used in experimental studies.

To summarize, we believe that using a novel technique of *ab initio* molecular dynamics directly tracing temporal polaron motion, we were able to address and answer the most fundamental and most important current questions pertinent to the charge transport in conducting polymers.

Paper III

In this paper, we discuss the growing demand for versatile, scalable, and affordable power sources for distributed microelectronics and sensors. Heat-harvesting organic thermoelectric generators (TEGs) are emerging as promising solutions for future energy needs. Recent advancements in organic thermoelectric materials have made these devices more practical, but challenges remain in designing and fabricating organic TEGs suitable for real-world applications.

Small sensors and wearable devices require micro-thermoelectric generators (μTEGs) with high power density and compact sizes. However, typical organic TEGs demonstrate fewer than 10 thermocouples (TCs) per cm^2. To address this, we propose a rolled, organic μTEG architecture that uses large-area, solution-based deposition techniques—such as inkjet printing and spray-coating—combined with an ultrathin parylene substrate. This design achieves a thermocouple density of 1842 TCs cm^{-2} and generates a power output of 0.15 μW cm^{-2} at a temperature difference (ΔT) of 50 K. Our finite element simulations support this architecture, indicating that power densities in the mW cm−2 range at ΔT = 10 K could be achieved with further design improvements and advancements in organic thermoelectric inks.

The μTEG architecture we propose takes advantage of in-plane, large-area fabrication techniques on micron-thin substrates and a rolling process to produce high-density thermocouples. We validated this architecture using PEDOT:PSS (p-type) and BBL:PEI (n-type) materials, which were applied using inkjet printing and spray-coating. This μTEG design achieves the highest thermocouple density ever reported for a fully organic TEG, at 1842 TCs cm^{-2}, while generating a power density of 0.15 μW cm^{-2} at ΔT = 50 K. Simulations revealed that with precise

fabrication, this device could achieve power densities exceeding 1 μW cm^{-2}.

Paper IV

Conducting polymers such as PEDOT are at the forefront of electronic and bioelectronic applications, yet their charge transport mechanisms remain challenging to predict and optimize because of inherent complexity of their structure and morphology. Our work provides a comprehensive experimental-theoretical investigation into how solvent post-treatment influences PEDOT:Tos thin-film morphology and electrical conductivity. By combining molecular dynamics, density functional theory, transport calculations, and experimental characterization (GIWAXS, XPS, and conductivity measurements), we establish a detailed structure-property relationship for these materials.

A key innovation of our study is the development of a machine learning (ML) framework that dramatically accelerates charge transport calculations. Specifically, we employ convolutional neural networks to predict transfer integrals directly from the Coulomb matrix, enabling efficient multi-scale mobility calculations. This represents a significant leap forward in computational materials science, allowing for the mobility calculations of polymer films at scales previously unattainable with excising conventional methods. By integrating ML with state-of-the-art experimental techniques, we not only validate our theoretical predictions but also provide a new paradigm for accelerating material design in the field of organic electronics.

While ML-driven predictions have gained significant traction in materials science, most studies remain theoretical and are still awaiting experimental confirmation. Our work, in contrast, overcomes this critical gap by providing direct experimental validation of ML-predicted conductivity trends, demonstrating that ML can be a powerful tool for guiding materials design and optimization. This unique combination of theory and experiment underscores the robustness and practical relevance of our approach.

Our findings are of broad interest to researchers in materials science, computational physics, and organic electronics. The ability to

systematically control and predict charge transport properties in conducting polymers opens new avenues for optimizing electronic and bioelectronic devices. Moreover, this work serves as a stepping stone for further ML applications in soft materials, potentially revolutionizing the way complex molecular systems are analyzed.

References

[1] A. Rezania and D. Davila Pineda, Eds., *Thermoelectric energy conversion: basic concepts and device applications*. in Advanced micro and nanosystems. Weinheim, Germany: Wiley-VCH, 2017. doi: 10.1002/9783527698110.

[2] F. Ritz and C. E. Peterson, "Multi-mission radioisotope thermoelectric generator (MMRTG) program overview," in *2004 IEEE Aerospace Conference Proceedings (IEEE Cat. No.04TH8720)*, Big Sky, MT, USA: IEEE, 2004, pp. 2950–2957. doi: 10.1109/AERO.2004.1368101.

[3] R. C. O'Brien, R. M. Ambrosi, N. P. Bannister, S. D. Howe, and H. V. Atkinson, "Safe radioisotope thermoelectric generators and heat sources for space applications," *Journal of Nuclear Materials*, vol. 377, no. 3, pp. 506–521, Jul. 2008, doi: 10.1016/j.jnucmat.2008.04.009.

[4] Y. Jia *et al.*, "Wearable Thermoelectric Materials and Devices for Self-Powered Electronic Systems," *Advanced Materials*, vol. 33, no. 42, p. 2102990, Sep. 2021, doi: https://doi.org/10.1002/adma.202102990.

[5] N. Pataki, P. Rossi, and M. Caironi, "Solution processed organic thermoelectric generators as energy harvesters for the Internet of Things," *Applied Physics Letters*, vol. 121, no. 23, p. 230501, Dec. 2022, doi: 10.1063/5.0129861.

[6] T.-P. Nguyen, *Organic Electronics 1: Materials and Physical Processes*. Newark: John Wiley & Sons, Incorporated, 2021.

[7] A. Elschner, *PEDOT: principles and applications of an intrinsically conductive polymer*. Boca Raton, FL: CRC Press, 2011.

[8] H. Shirakawa, "The discovery of polyacetylene film," *Synthetic Metals*, vol. 125, no. 1, pp. 3–10, Nov. 2001, doi: 10.1016/S0379-6779(01)00507-0.

[9] G. Inzelt, *Conducting polymers: a new era in electrochemistry*, 2nd ed. in Monographs in electrochemistry. Heidelberg ; New York: Springer, 2012.

[10] A. Troisi, D. L. Cheung, and D. Andrienko, "Charge Transport in Semiconductors with Multiscale Conformational Dynamics," *Phys. Rev. Lett.*, vol. 102, no. 11, p. 116602, Mar. 2009, doi: 10.1103/PhysRevLett.102.116602.

[11] A. Troisi and D. L. Cheung, "Transition from dynamic to static disorder in one-dimensional organic semiconductors," *The Journal of Chemical Physics*, vol. 131, no. 1, p. 014703, Jul. 2009, doi: 10.1063/1.3167406.

[12] W. P. Su, J. R. Schrieffer, and A. J. Heeger, “Solitons in Polyacetylene,” *Phys. Rev. Lett.*, vol. 42, no. 25, pp. 1698–1701, Jun. 1979, doi: 10.1103/PhysRevLett.42.1698.
[13] K. Hannewald, V. M. Stojanović, J. M. T. Schellekens, P. A. Bobbert, G. Kresse, and J. Hafner, “Theory of polaron bandwidth narrowing in organic molecular crystals,” *Phys. Rev. B*, vol. 69, no. 7, p. 075211, Feb. 2004, doi: 10.1103/PhysRevB.69.075211.
[14] H. Oberhofer, K. Reuter, and J. Blumberger, “Charge Transport in Molecular Materials: An Assessment of Computational Methods,” *Chem. Rev.*, vol. 117, no. 15, pp. 10319–10357, Aug. 2017, doi: 10.1021/acs.chemrev.7b00086.
[15] R. P. Fornari and A. Troisi, “Theory of charge hopping along a disordered polymer chain,” *Phys. Chem. Chem. Phys.*, vol. 16, no. 21, p. 9997, 2014, doi: 10.1039/c3cp54661f.
[16] R. A. Marcus, “On the Theory of Electron-Transfer Reactions. VI. Unified Treatment for Homogeneous and Electrode Reactions,” *The Journal of Chemical Physics*, vol. 43, no. 2, pp. 679–701, Jul. 1965, doi: 10.1063/1.1696792.
[17] A. Miller and E. Abrahams, “Impurity Conduction at Low Concentrations,” *Phys. Rev.*, vol. 120, no. 3, pp. 745–755, Nov. 1960, doi: 10.1103/PhysRev.120.745.
[18] Friedrich JonasGerhard HeywangWerner SchmidtbergJurgen HeinzeMichael, “Polythiophenes, process for their preparation and their use”
[19] M. Donoval *et al.*, “Relation between secondary doping and phase separation in PEDOT:PSS films,” *Applied Surface Science*, vol. 395, pp. 86–91, Feb. 2017, doi: 10.1016/j.apsusc.2016.05.076.
[20] Z. Zhu, L. Wang, and C. Gao, “Thermoelectric properties of PEDOTs,” in *Advanced PEDOT Thermoelectric Materials*, Elsevier, 2022, pp. 73–95. doi: 10.1016/B978-0-12-821550-0.00011-1.
[21] S. Garreau, G. Louarn, J. P. Buisson, G. Froyer, and S. Lefrant, “In Situ Spectroelectrochemical Raman Studies of Poly(3,4-ethylenedioxythiophene) (PEDT),” *Macromolecules*, vol. 32, no. 20, pp. 6807–6812, Oct. 1999, doi: 10.1021/ma9905674.
[22] M. V. Fabretto *et al.*, “Polymeric Material with Metal-Like Conductivity for Next Generation Organic Electronic Devices,” *Chem. Mater.*, vol. 24, no. 20, pp. 3998–4003, Oct. 2012, doi: 10.1021/cm302899v.
[23] B. J. Worfolk *et al.*, “Ultrahigh electrical conductivity in solution-sheared polymeric transparent films,” *Proc. Natl. Acad. Sci. U.S.A.*, vol. 112, no. 46, pp. 14138–14143, Nov. 2015, doi: 10.1073/pnas.1509958112.

[24] E. Maciá, Ed., *Thermoelectric materials: advances and applications*. Boca Raton, Fla: Pan Stanford, 2015.
[25] L. Chen, R. Liu, and X. Shi, *Thermoelectric materials and devices*. Amsterdam: Elsevier, 2021.
[26] M. V. Vedernikov and E. K. Iordanishvili, "A.F. Ioffe and origin of modern semiconductor thermoelectric energy conversion," in *Seventeenth International Conference on Thermoelectrics. Proceedings ICT98 (Cat. No.98TH8365)*, Nagoya, Japan: IEEE, 1998, pp. 37–42. doi: 10.1109/ICT.1998.740313.
[27] S. Wang *et al.*, "The realization of a high thermoelectric figure of merit in Ge-substituted β-Zn4Sb3 through band structure modification," *J. Mater. Chem.*, vol. 22, no. 28, p. 13977, 2012, doi: 10.1039/c2jm30906h.
[28] L.-D. Zhao *et al.*, "Ultralow thermal conductivity and high thermoelectric figure of merit in SnSe crystals," *Nature*, vol. 508, no. 7496, pp. 373–377, Apr. 2014, doi: 10.1038/nature13184.
[29] B. Qin *et al.*, "High thermoelectric efficiency realized in SnSe crystals via structural modulation," *Nat Commun*, vol. 14, no. 1, p. 1366, Mar. 2023, doi: 10.1038/s41467-023-37114-7.
[30] O. Bubnova *et al.*, "Optimization of the thermoelectric figure of merit in the conducting polymer poly(3,4-ethylenedioxythiophene)," *Nature Mater*, vol. 10, no. 6, pp. 429–433, Jun. 2011, doi: 10.1038/nmat3012.
[31] L. Zhang, T. Wang, Z. Shen, and M. Liu, "Chiral Nanoarchitectonics: Towards the Design, Self-Assembly, and Function of Nanoscale Chiral Twists and Helices," *Advanced Materials*, vol. 28, no. 6, pp. 1044–1059, Feb. 2016, doi: 10.1002/adma.201502590.
[32] W. Zhao, J. Ding, Y. Zou, C. Di, and D. Zhu, "Chemical doping of organic semiconductors for thermoelectric applications," *Chem. Soc. Rev.*, vol. 49, no. 20, pp. 7210–7228, 2020, doi: 10.1039/D0CS00204F.
[33] Y. Sun, C. Di, W. Xu, and D. Zhu, "Advances in n-Type Organic Thermoelectric Materials and Devices," *Adv Elect Materials*, vol. 5, no. 11, p. 1800825, Nov. 2019, doi: 10.1002/aelm.201800825.
[34] F. Jiang, C. Liu, and J. Xu, Eds., *Advanced PEDOT thermoelectric materials*. in Woodhead Publishing series in electronic and optical materials. Duxford, United Kingdom Cambridge, MA: Woodhead Publishing, 2022.
[35] J. Y. Kim, J. H. Jung, D. E. Lee, and J. Joo, "Enhancement of electrical conductivity of poly(3,4-ethylenedioxythiophene)/poly(4-styrenesulfonate) by a change of

solvents," *Synthetic Metals*, vol. 126, no. 2–3, pp. 311–316, Feb. 2002, doi: 10.1016/S0379-6779(01)00576-8.
[36] J. Feng-Xing, X. Jing-Kun, L. Bao-Yang, X. Yu, H. Rong-Jin, and L. Lai-Feng, "Thermoelectric Performance of Poly(3,4-ethylenedioxythiophene): Poly(styrenesulfonate)," *Chinese Phys. Lett.*, vol. 25, no. 6, pp. 2202–2205, Jun. 2008, doi: 10.1088/0256-307X/25/6/076.
[37] G.-H. Kim, L. Shao, K. Zhang, and K. P. Pipe, "Engineered doping of organic semiconductors for enhanced thermoelectric efficiency," *Nature Mater*, vol. 12, no. 8, pp. 719–723, Aug. 2013, doi: 10.1038/nmat3635.
[38] L. Chen, R. Liu, and X. Shi, "General principles of thermoelectric technology," in *Thermoelectric Materials and Devices*, Elsevier, 2021, pp. 1–18. doi: 10.1016/B978-0-12-818413-4.00001-6.
[39] L. Francioso *et al.*, "PDMS/Kapton Interface Plasma Treatment Effects on the Polymeric Package for a Wearable Thermoelectric Generator," *ACS Appl. Mater. Interfaces*, vol. 5, no. 14, pp. 6586–6590, Jul. 2013, doi: 10.1021/am401222p.
[40] Y. Li, X. Wang, D. Luo, Y. Shi, Y. Ren, and Y. Yan, "Recent development in structural designs and thermal enhancement technologies of thermoelectric generator with different types of heat sources: A review," *e-Prime - Advances in Electrical Engineering, Electronics and Energy*, vol. 4, p. 100180, Jun. 2023, doi: 10.1016/j.prime.2023.100180.
[41] D. C. Rapaport, *The art of molecular dynamics simulation*, Second edition. Cambridge, UK New York, NY: Cambridge University Press, 2004.
[42] K. Zhou and B. Liu, *Molecular dynamics simulation: fundamentals and applications*. Amsterdam Oxford Cambridge: Elsevier, 2022.
[43] A. P. Thompson *et al.*, "LAMMPS - a flexible simulation tool for particle-based materials modeling at the atomic, meso, and continuum scales," *Computer Physics Communications*, vol. 271, p. 108171, Feb. 2022, doi: 10.1016/j.cpc.2021.108171.
[44] R. Car and M. Parrinello, "Unified Approach for Molecular Dynamics and Density-Functional Theory," *Phys. Rev. Lett.*, vol. 55, no. 22, pp. 2471–2474, Nov. 1985, doi: 10.1103/PhysRevLett.55.2471.
[45] D. Marx and J. Hutter, *Ab initio molecular dynamics: basic theory and advanced methods*. Cambridge: Cambridge University Press, 2009. doi: 10.1017/CBO9780511609633.
[46] S. S. Iyengar, H. B. Schlegel, and G. A. Voth, "Atom-Centered Density Matrix Propagation (ADMP): Generalizations Using

Bohmian Mechanics," *J. Phys. Chem. A*, vol. 107, no. 37, pp. 7269–7277, Sep. 2003, doi: 10.1021/jp034633m.
[47] S. M. Musa, A. V. Kulkarni, and V. K. Havanur, *Finite element analysis: a primer*. Dulles, Virginia: Mercury Learning and Information, 2014.
[48] M. Weiser, *Inside Finite Elements*. De Gruyter, 2016. doi: 10.1515/9783110373202.
[49] J. S. Gero and F. Sudweeks, *Artificial Intelligence in Design '96*. Dordrecht: Springer Netherlands, 1996. doi: 10.1007/978-94-009-0279-4.
[50] Z.-H. Zhou, *Machine learning*. Singapore: Springer, 2021.
[51] V. Gupta, *Mastering Machine Learning: Practical Applications Across Industries*. Vijay Gupta, 2024.
[52] A. Lindholm, *Machine learning: a first course for engineers and scientists*. Cambridge, UK ; New York, NY: Cambridge University Press, 2022.
[53] I. Goodfellow, Y. Bengio, and A. Courville, *Deep learning*. in Adaptive computation and machine learning. Cambridge, Mass: The MIT press, 2016.
[54] C. C. Aggarwal, *Neural Networks and Deep Learning: A Textbook*. Cham: Springer International Publishing AG, 2018.
[55] "Materials Genome Initiative." [Online]. Available: https://www.mgi.gov/
[56] P. Raccuglia *et al.*, "Machine-learning-assisted materials discovery using failed experiments," *Nature*, vol. 533, no. 7601, pp. 73–76, May 2016, doi: 10.1038/nature17439.
[57] "Harvard Clean Energy Project." [Online]. Available: http://cepdb.molecularspace.org/
[58] "Open Quantum Materials Database." [Online]. Available: http://oqmd.org/
[59] "Materials Project." [Online]. Available: https://materialsproject.org/
[60] K. Choudhary, I. Kalish, R. Beams, and F. Tavazza, "High-throughput Identification and Characterization of Two-dimensional Materials using Density functional theory," *Sci Rep*, vol. 7, no. 1, p. 5179, Jul. 2017, doi: 10.1038/s41598-017-05402-0.
[61] A. Merchant, S. Batzner, S. S. Schoenholz, M. Aykol, G. Cheon, and E. D. Cubuk, "Scaling deep learning for materials discovery," *Nature*, vol. 624, no. 7990, pp. 80–85, Dec. 2023, doi: 10.1038/s41586-023-06735-9.
[62] J. Lederer, W. Kaiser, A. Mattoni, and A. Gagliardi, "Machine Learning–Based Charge Transport Computation for Pentacene,"

Advcd Theory and Sims, vol. 2, no. 2, p. 1800136, Feb. 2019, doi: 10.1002/adts.201800136.
[63] O. Çaylak, A. Yaman, and B. Baumeier, "Evolutionary Approach to Constructing a Deep Feedforward Neural Network for Prediction of Electronic Coupling Elements in Molecular Materials," *J. Chem. Theory Comput.*, vol. 15, no. 3, pp. 1777–1784, Mar. 2019, doi: 10.1021/acs.jctc.8b01285.
[64] C.-I. Wang, M. K. E. Braza, G. C. Claudio, R. B. Nellas, and C.-P. Hsu, "Machine Learning for Predicting Electron Transfer Coupling," *J. Phys. Chem. A*, vol. 123, no. 36, pp. 7792–7802, Sep. 2019, doi: 10.1021/acs.jpca.9b04256.
[65] M. Rinderle, W. Kaiser, A. Mattoni, and A. Gagliardi, "Machine-Learned Charge Transfer Integrals for Multiscale Simulations in Organic Thin Films," *J. Phys. Chem. C*, vol. 124, no. 32, pp. 17733–17743, Aug. 2020, doi: 10.1021/acs.jpcc.0c04355.
[66] P. Friederich, S. León, J. D. Perea, L. M. Roch, and A. Aspuru-Guzik, "The influence of sorbitol doping on aggregation and electronic properties of PEDOT:PSS: a theoretical study," *Mach. Learn.: Sci. Technol.*, vol. 2, no. 1, p. 01LT01, Mar. 2021, doi: 10.1088/2632-2153/ab983b.

Papers

The papers associated with this thesis have been removed for copyright reasons. For more details about these see:

https://doi.org/10.3384/9789181180787

FACULTY OF SCIENCE AND ENGINEERING

Linköping Studies in Science and Technology, Dissertation No. 2446, 2025
Department of ITN

Linköping University
SE-581 83 Linköping, Sweden

www.liu.se

LINKÖPING UNIVERSITY